Physica D 43 (1990) 229–268
North-Holland

TRANSPORT RATES OF A CLASS OF TWO-DIMENSIONAL MAPS AND FLOWS

V. ROM-KEDAR
The James Franck Institute and The Computational and Applied Mathematics Program, Mathematical Disciplines Center, University of Chicago, Chicago, IL 60637, USA

Received 25 September 1989
Revised manuscript received 29 January 1990
Accepted 29 January 1990
Communicated by R.S. MacKay

A method is developed for estimating the transport rates of phase space areas for a class of two-dimensional diffeomorphisms and flows. The class of diffeomorphisms we consider are defined by the topological structure of their stable and unstable manifolds, and hence are universal. We show how to estimate the transport rates for a class of diffeomorphisms found by Easton and for an extension of this class of diffeomorphisms which is found via a "perturbation" of the topology of the stable and unstable manifolds. This is done by introducing symbolic dynamics and transfer matrices which in turn relate transport phenomena in phase space to Markov processes in a precise manner. In addition to the transport rates, we use the transfer matrices to obtain estimates for the topological entropy, averaged stretching rates, and the elongation rate of the unstable manifold. The flows we consider are two-dimensional, time-periodic flows which can be reduced via a Poincaré section to the extended family of maps. We develop an analytical method, based on Chirikov's Whisker map, to classify a given flow according to the structure of its manifolds in its Poincaré section. This allows the techniques developed here for maps to be directly applied to time-periodic flows.

1. Introduction

The study of transport phenomena is important in a variety of diverse fields, e.g. fluid flows [1–3], plasma flows [4], mechanics [5, 6] and chemistry [7, 8]. In many applications the transport of quantities in the physical space can be related to transport of area (or volume) in phase space of a diffeomorphism. For example, the transport rates of a passive scalar in a time-periodic fluid flow is given by the transport rates of area (or volume) in the Poincaré map induced by the ODEs describing the particle motion [1–3].

In previous works on transport in two-dimensional phase space various statistical methods to describe the particles motion were used, the philosophy being that the stochastic motion which is typical to two-dimensional maps inhibits exact solutions to the transport equations. Subsequently, several authors have discovered that the flux mechanism between regions in phase space which are bounded by segments of stable and unstable manifolds is quite simple, and can be approximated by various methods [3, 4, 9]. Recently, it was shown that in a large class of two-dimensional diffeomorphisms the transport rates are given in terms of the distribution of specific small regions in phase space ("lobes") in time (see ref. [10], hereafter called RW), hence that the statistical methods developed so far assumed many more degrees of freedom than appropriate. These ideas were used to compute the transport rates of a passive scalar in a specific two-dimensional, time-periodic fluid flow (see ref. [3], hereafter called RLW), and were generalized to higher dimensions [11]. The main drawback in applying the above theory was the lack of

0167-2789/90/$03.50 © Elsevier Science Publishers B.V.
(North-Holland)

an efficient method for estimating the distribution of the lobes in phase space. In this paper I develop a method for approximating these quantities in a family of diffeomorphisms. This family is less general than the one treated in RW; however, the same approach should lead to similar results for the general case as well as the higher-dimensional generalizations.

The starting point of this paper is a work by Easton [12]. Easton classified a family of trellises by their initial developments as defined by an integer parameter l. (The development of a trellis is the figure formed by two finite segments, one segment of the stable manifold and one of the unstable manifold. The segments end points are given by the fixed point and a "simple" homoclinic point, termed a "pip". Figs. 1–8 are drawings of the developments of various trellises.) Easton named this family of trellises "type-l trellises", with $l \in \mathbb{Z}^+$. He showed that his classification is well defined in the sense that the developments of two trellises of type l are homeomorphic. In this paper we associate with each class of type-l diffeomorphisms (diffeomorphisms which attain type-l trellises) symbolic dynamics and hence a transition matrix. We show that in addition to the usual consequences of this definition one gets quantitative estimates for the distribution of the lobes in phase space, which in turn give the desired transport rates and their asymptotic behavior. The estimates involved in these calculations are semi-linear approximations to the topology of the trellises which can be improved using techniques introduced by Gaspard and Rice in a similar context [7]. Judd [13] has recently developed, using graph theory, a method to estimate the fractal dimension of a homoclinic bifurcation using similar ideas to those presented in Easton's work and here. His work is more general as far as the class of trellises he considers and may be used as a guide line for generalizing the present work to include more cases and different geometries.

Examining more carefully the development of the stable and unstable manifolds, one concludes that a complete classification of the trellises requires a countable infinity of integer parameters. This reclassification can be thought of as a generalization of Easton's classification to type-**l** trellises where **l** is an infinite series of integers. Moreover, if one considers the trellises of a family of two-dimensional diffeomorphisms depending on one real-valued parameter μ, one expects to find a measure zero and sparse set of parameter values for which the trellises are of type **l** (for any given series **l**). Specifically, the set of parameters for which the trellises are of type-l is of measure zero and is non-dense, hence the type-l trellises are not structurally stable. Nonetheless, one would hope that in the μ-neighborhood of the parameter values for which the trellises are of type l the estimates, given in this paper, of the transport rates, the stretching rates and the manifold length will be valid. Evidence supporting this assertion is one of the main results of this paper. A proof for such an assertion requires the full classification of the trellises in the neighborhood of a type-l trellis, which is beyond the scope of this paper. Instead, we generalize Easton's trellises and obtain a series of trellises which converge topologically to the type-l trellises. The simplest generalization of Easton's trellises is obtained by adding two more integer parameters to the trellis classification. We associate symbolic dynamics and transition matrices with this broadened class of diffeomorphism. Then, we show that indeed all the quantitative characteristics of this family of trellises asymptote, in an exponential rate in the two new parameters, to the ones of the type-l trellises. Hence, the initial development of the manifold can be used to estimate the transport rates and the error reduces exponentially with the level of the initial development. Application of the above ideas to a specific flow will be given in a subsequent paper.

Using the transition matrices we obtain a natural relation between transport phenomena in two-dimensional maps and Markov's chains. We suggest a new statistical approach to the computation of the diffusion rate which employs the structure of the stable and unstable manifolds.

Finally, we obtain a complete analytical method for calculating the transport rates of a family of two-dimensional, time-periodic flows. The trellises associated with the flows are the trellises of their

induced Poincaré maps. We use Chirikov's [14] Whisker map to approximate the characteristic parameters (such as l) of these trellises as well as the first few escape rates of the Poincaré maps. Given these parameters and the first few escape rates, the techniques developed above for maps can be utilized.

This paper is organized as follows; in section 2 we describe Easton's trellises. In section 3 we construct the symbolic dynamics and the transition matrices associated with these trellises and derive estimates for the transport rates of areas in phase space under the maps associated with Easton's trellises. In section 4 we define a broader class of trellises and in section 5 we construct their symbolic dynamics and calculate their escape rates. Section 6 is devoted for the estimates of the length of the manifold development for the various cases. In section 7 we show that if two developments agree for a long time, their escape rates and their topological structures are asymptotically close. In section 8 we relate the above description of transport in phase space to Markov's chains. In section 9 we derive an analytical method to approximate the initial development of the trellis associated with two-dimensional time-periodic flows.

2. Easton's trellises

Easton called the figure formed by the transversal intersecting stable and unstable manifolds of a hyperbolic fixed point on a 2-manifold a trellis. As was noted by Poincaré [15] 97 years ago, the trellis has in general an incredibly complex structure, which reflects the chaotic dynamics associated with the dynamical system producing the trellis. Easton was the first to realize that though in general the structure is complex, there are underlying rules for the development of the trellis. These rules are determined in general by a countable infinity of integer parameters, hence they are hard to formulate. Easton has constructed a family of trellises which obey the simplest possible rules, using only one integer parameter l. We now describe the family of type-l trellises found by Easton. Since Easton's results are the basis for this paper, I devote this section to describing them.

The formation of a type-l trellis is described in a sequence of steps. Suppose p is a hyperbolic fixed point and denote its two branches of the stable (unstable) manifolds by W^s_+, W^s_- (W^u_+, W^u_-), see fig. 1.

Definition 1.1. A point q_0 in phase space is called *homoclinic point* if it belongs to both the stable and unstable manifolds of p.

Definition 1.2. A homoclinic point q_0 is called a *primary intersection point* (*pip*) if the segments of the stable and unstable manifolds connecting the fixed point p to q_0, denoted by $S[p, q_0]$, $U[p, q_0]$

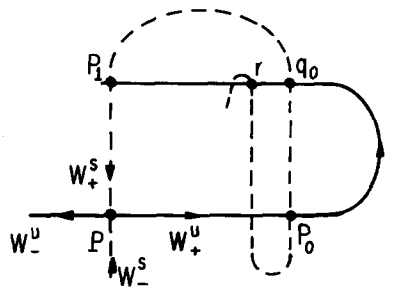

Fig. 1. The definition of a pip. In this figure, and in figs. 2–8 and 15 we use the following notation: p denotes the fixed point. ——— denotes the stable manifold of p. ——— denotes the unstable manifold of p. q_0 and p_0 are pip's, r is not a pip.

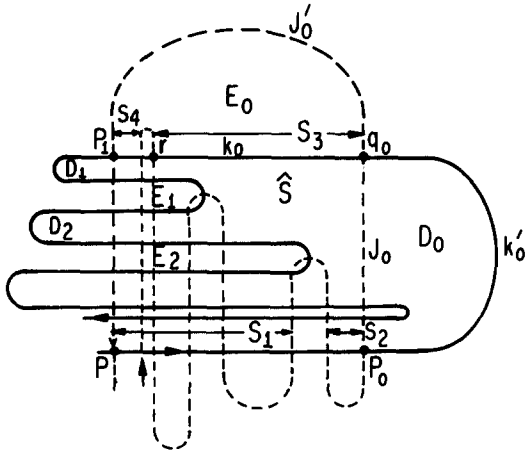

Fig. 2. The geometry of a type-l trellis. In this figure $l = 3$.

respectively, intersect only in p and q_0 (see fig. 1). The pip orbit of q_0 is the set $\{q_i\}$, $i \in \mathbb{Z}$, where q_i is the ith image of q_0 under the map.

Following Easton, we make three assumptions about the manifold structure.

Hypothesis A. W^u_+ contains exactly two pip orbits denoted by $\{p_i\}, \{q_i\}$, $i \in \mathbb{Z}$, where $p_i \in S[q_i, q_i - 1]$.

We define the segments of W^u_+ and W^s_+ with end points p_i, q_i as follows (see fig. 2):

$$J_i = S[q_i, p_i], \qquad J'_i = S(p_{i+1}, q_i), \qquad K_i = U[q_i, p_{i+1}], \qquad K'_i = U(p_i, q_i). \tag{1}$$

Clearly, $R_n = F^n(R_0)$, where R stands for any of the segments J, K, J', K' and F denotes the diffeomorphism. Moreover, $W^u_+ = \bigcup_{n=-\infty}^{\infty} K_n \cup K'_n$, and similarly $W^s_+ = \bigcup_{n=-\infty}^{\infty} J_n \cup J'_n$.

Hypothesis B. The sequences $\{K'_n\}$ and $\{J'_{-n}\}$ are sequences of arcs which accumulate along W^u_- and W^s_-, respectively, for all $n > 0$. W^s_- and W^u_- do not contain any homoclinic points, and the only homoclinic points contained in these arcs are the pips.

Let D_r denote the region bounded by J_r and K'_r and E_r the region bounded by K_r and J'_r. We will call these regions "lobes" and we refer to the family of the E_r (D_r) lobes as the E (D) lobes. As was shown in RW, the evolution of the lobes determines the escape rates from the region bounded by $S[p, p_0]$ and $U[p, p_0]$, which we denote by $\hat{S}$, see fig. 2. For future reference we denote the region $\hat{S} - E_0$ by S.

Hypotheses A and B are made so as to consider the simplest possible geometry and are satisfied by a large family of diffeomorphisms. For example, the Poincaré map of a particle in a cubic potential with time-periodic forcing will result in such a configuration. The first hypothesis is not essential and is made just for the convenience of notation. On the other hand the second hypothesis is crucial for simplifying the form of the trellis. Cases in which the second assumption is dropped are under current investigation. A similar approach to the one presented here should work; however, the classification process seems to be much harder.

The next hypothesis classifies the trellises according to the nature of the intersection between the arcs J_n and K_m for various n, m. Note that a trellis is defined uniquely by the intersection matrix

$$M(n,m) = J_n \cap K_m = F^m(J_{n-m} \cap K_0) = F^m(M(n-m, 0)), \tag{2}$$

which consists of all the homoclinic points and their *ordering* along the stable and unstable manifolds; the homoclinic points can be ordered by their distance from the fixed point along the stable or unstable manifolds, resulting in the *stable ordering* and the *unstable ordering*, respectively, i.e. $a <_u b$ means that $U[p,a] \subset U[p,b]$ and similarly for $<_s$. For example, in fig. 1 $p_0 <_u q_0 <_u r <_u p_1$ where $p_1 <_s q_0 <_s p_0 <_s r$. The term $M(n,m)$ consists of a set of $r(n,m)$ points ordered by the unstable ordering and a set of $r(n,m)$ integers, denoted by $I(n,m)$, which maps the unstable ordering to the stable one. It follows from eq. (2) that once $r(n,0)$ and $I(n,0)$ are determined for all n, $r(n,m)$ and $I(n,m)$ are determined for all n,m. Since two trellises are topologically conjugate with a homeomorphism which preserves both the stable and unstable orderings (weakly equivalent in Easton's terminology) iff they have the same matrices r and I, a complete classification of the trellises to topological conjugacy classes requires in general a *countable infinity* of integer parameters corresponding to the terms $r(n,0)$ and $I(n,0)$. The third hypothesis on the trellis development is restrictive enough so that the intersection matrix is completely determined by one integer parameter l. In fact, this hypothesis supplies a recursion relation (which depends on the parameter l) for the terms of $r(n,0)$ and $I(n,0)$. First, one assumes that E_l is the first E lobe which intersects the D lobes, and that this intersection is the simplest possible, namely a two-point intersection, as shown in fig. 2 (a more complicated intersection of E_l with D_0 is shown in fig. 5 and is discussed in section 3). Then, one determines the higher-order intersections (larger n,m) by allowing only the necessary intersections to occur. The second step can be formulated in a precise manner using the notion of transition numbers.

Definition 1.3. The homoclinic point $q \in K_0 \cap J_{-t(q)}$ has a *transition number* $t(q) \in \mathbb{Z}^+$.

For example, in fig. 2 the homoclinic point r has a transition number 3. Let h_n denote all the homoclinic points $q \in K_0$ with $1 \le t(q) \le n$.

Hypothesis C. There exists a positive integer l such that if a,b are two $<_u$ adjacent points of h_n then

(1) If $t(a) = t(b)$ then $U[a,b]$ is contained in $D_{-t(a)}$.

(2) If $t(a) < t(b)$ then $U[a,b] \cap J_{-(n+1)}$ contains exactly two points whenever $n - t(a) \ge l$ and is empty whenever $n - t(a) < l$.

Definition 1.4. A trellis which satisfies hypotheses A, B and C is called a trellis of type l.

In fig. 2 we draw the initial development of a type-3 trellis. In general, given that E_l is the first E lobe to intersect D_0, the terms of $r(n,m)$ are bounded from below by the corresponding terms of a type-l trellis matrix $r_l(n,m)$; new homoclinic points not resulting from the intersection of E_l and D_0 may appear in $M(n,m)$.

Hypotheses A, B and C allow one to get a complete description of the topology of the type-l trellis. Moreover, Easton has shown that this classification is well defined since two trellises of type l have homeomorphic developments; the sets $\bigcup_{-\infty}^{n}(K_j \cup K_j')$ are homeomorphic for all (finite) n and similarly for the stable manifold development. Easton has also calculated the number of homoclinic points created at every step of the development. In section 3 we associate with every type-l trellis symbolic dynamics and a transition matrix. This formulation enables us to compute the number of homoclinic points created every iteration ($r(n,m)$), to approximate the area ejected out every iteration and to approximate topological properties such as the topological entropy.

As Easton himself indicated, the above hypotheses restrict the class of diffeomorphism considerably. I would even conjecture that a family of two-dimensional diffeomorphism depending on a real parameter μ will generically attain a measure zero, sparse set of parameters μ for which the trellises satisfy hypothesis C for some integer l, hence that the type-l trellises are not structurally stable. The basis for this conjecture is that arbitrarily close to a parameter value μ for which hypothesis C is satisfied there exists a value μ_t for which the trellis attains a homoclinic tangency, violating hypothesis C. Moreover, this hypothesis is violated (generically) in the semi-open interval $[\mu_t, \mu_t \pm \epsilon)$ for some $\epsilon > 0$ and not necessarily small (+ sign if $\mu_t > \mu$, − sign if $\mu_t < \mu$). In this paper we will show that nevertheless the type-l trellises are important in applications, since

(a) One can easily estimate important quantities such as the Escape rates, the Topological entropy and the manifold Length (the ETL) of a type-l trellis.

(b) The class of type-l trellises and the methods for estimating the ETL can be broadened in a consistent fashion to a larger class of trellises, supplying better approximations to the topology and the ETL of a general trellis.

(c) If the topology and the metric properties of a general trellis are "sufficiently close" to the one of a type-l trellis, its ETL can be approximated by the ETL of the type-l trellis.

3. Symbolic dynamics for type-l trellises

As Easton noted, a type-1 trellis is homeomorphic to a Smale horseshoe map [16–18]. For this map, the construction of symbolic dynamics is well known. Moreover, the computation of the topological entropy, the number of periodic orbits, the number of homoclinic orbits and the escape rates is straightforward. We start by formalizing the relation between all these quantities, the transition matrix and the weighted transition matrix for the horseshoe map and then we generalize these ideas to a type-l trellis.

3.1. Type-1 trellis

We associate with the type-1 trellis, with the initial development as drawn in fig. 3 symbolic dynamics as follows: Define a horizontal strip to be a topologically rectangular region for which one edge is contained in J_0 and another is contained in J_n for some $n > 0$. Identify the horizontal strips H_1 and H_2

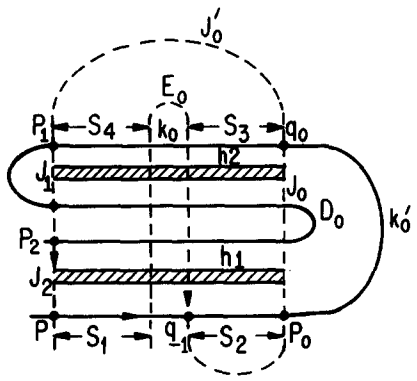

Fig. 3. The geometry of a type-1 trellis – a horseshoe.

as the regions bounded by J_2, K_{-1}, J_0, K_1 and J_1, K_1, J_0, K_0, respectively. Denote a horizontal strip which is contained in H_i by h_i for $i = 1, 2$. Then it is easy to see that the following diagram describes the action of any map which has a type-1 trellis on horizontal strips:

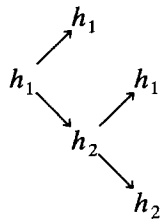

(3)

Given this diagram one can label each strip by a sequence of 1, 2 which describes the strip position under the map, namely $h_{s_0,\ldots,s_k} \in \{1,2\}$ is a horizontal strip in H_{s_k} which is a component of the kth image of a strip in H_{s_0}. We can associate a transition matrix with this labeling, which in this case is given trivially by

$$T_1 = \begin{pmatrix} 1 & 1 \\ 1 & 1 \end{pmatrix}. \tag{4}$$

Similarly, one can define vertical strips and the vertical regions V_i, $i = 1, 2$ and construct labeling for the vertical strips as before. Replacing the h's with v's in diagram (3) will result in the action of the inverse map on the vertical strips. Using the relation $F(V_i) = H_i$, $i = 1, 2$ one can then combine the labeling of the vertical and horizontal strips to obtain labeling to rectangles by a two-sided series, which in the limit of infinite thin strips become a labeling of points in the invariant set of the map by a bi-infinite sequence of 1's and 2's [16–18].

Using the transition matrix we can find easily the following topological properties of a type-1 trellis:

(a) Number of horizontal strips in H_i, $i = 1, 2$ after n iterations: given the vector v^0 of initial number of strips in H_i, $i = 1, 2$, the number of strips after the nth iteration is given by v^n:

$$v^n = v^0 T_1^n = v^0 2^{n-1} T_1 = 2^{n-1} |v^0| (1,1), \quad n > 0, \tag{5}$$

where $|v|$ denotes the sum of the components of the vector v. In other words, since there is a one-to-one correspondence between labeling of horizontal strips and the allowed sequences of 1's and 2's [16, 18] one gets that the number of strips is amplified exactly as the number of allowed sequences, which in this case is given by 2^n.

(b) Number of points in $J_0 \cap K_n$, $r(0, n)$: using eq. (5), the observation that the horizontal strips h_1 and h_2 interest J_0 at exactly two points and that K_2 contains exactly two horizontal strips $h_1 \cup h_2$, we obtain

$$r(0,1) = 2, \qquad r(0,n) = (2,2) T_1^{n-2} (1,1)^{\mathrm{T}} = 2^n, \quad 2 \le n \tag{6}$$

and by construction we also establish that the number of strips of $F^n E \cap S$ is given by $r(0, n)/2 = 2^{n-1}$.

(c) The asymptotic exponential growth rate of the length K_n is given by the exponential growth rate of the number of horizontal strips created by E_n, hence is given by $\log 2$. This quantity supplies a lower bound on the topological entropy, as defined by Finn and Ott [19] for area-preserving maps. We conjecture that this is a sharp lower bound, as is the case for dissipative maps [13] and will define the asymptotic exponential growth rate to be the topological entropy. The topological entropy supplies a first

estimate to the length of the boundary of E_n, $L(K_n) \approx 2^n L(K_0)$, hence to the length of the development of W_+^u, $L(W_{+,n}^u)$. Section 6 is dedicated to the computation of sharper lower and upper bounds on $L(K_n)$ for finite n's.

(d) Number of periodic points: since there exists a homeomorphism between the shift map on the bi-infinite series of 1's and 2's and the horseshoe map [16–18] (restricted to the invariant set), the number of periodic orbits of period k is given by the number of allowed periodic sequences of 1's and 2's, which is given by $\mathrm{tr}(T_1^k)$ (see for example ref. [18]) hence is given by 2^k.

Note that in the dissipative case, when a strange attractor exists, the topological entropy can be defined also as the exponential growth rate of the number of periodic points of period k [20]. In general, it is not clear whether the amount of stretching of the manifold and the growth rate of the number of periodic orbits is so closely related in the area-preserving case. For the horseshoe map, it is obvious from (c) and (d) that they are equal. For a general type-l trellis, we will obtain results regarding the stretching of the manifold but not regarding the periodic orbits, hence this question remains open.

For $l > 1$ we cannot construct the analogous two-sided symbol sequence which is topologically conjugate, together with the shift map, to the dynamics of the map on the invariant set. Instead, we construct a one-sided sequence, describing the future (past) of horizontal (vertical) strips. It is therefore important to observe that the existence of the bi-infinite sequence of symbols was used only for the calculation of the number of periodic orbits. All the other results depend on one side of this sequence only, namely the relation $F(H_i) = V_i$ is not used in items (a)–(c).

3.2. *Escape rate computation for the horseshoe*

We now start with some new work regarding the horseshoe map. To obtain metric properties such as the escape rates and the distribution of the Lyapunov exponents on K_0, one can assign weights to the transition matrix T_1 which will be determined by the metric properties of the initial development of the trellis. Let W_1 be the weighted transition matrix:

$$W_1 = \begin{pmatrix} s_1 & s_2 \\ s_3 & s_4 \end{pmatrix}.$$

Geometrically, the terms of this matrix determine what portion of the area of the strip h_i is mapped to h_j for $i, j = 1, 2$. If the shape of S is rectangular (as depicted in all our figures) the s_i's are given by $s_i = S_i / L(K_0)$, where S_i are as shown in fig. 3. We will soon replace the action of the nonlinear map on the horizontal strips by the action of the matrix W_1 on their areas. The approximation involved in such a replacement is a semi-linear one, which can be justified if the horizontal and vertical strips are of approximately constant width. We will use a similar approach to approximate the escape rates of the type-l trellises and the broadened family of trellises defined in section 4. In all these cases one can improve the semi-linear approximation by considering more symbols as in the work of Gaspard and Rice [7] on the scattering from a classical chaotic repellor.

The crucial observation which permits us to proceed is that the weighted transition matrix can be used to approximate what portion of the area of a horizontal strip remains in S. Let a_1 denote the area of a strip h_1. The area of the strips h_{11}, h_{12} is given by $a_1 W_1(1,1)$ and $a_1 W_1(2,1)$ respectively, and in general the area of a strip $h_{s_0,\ldots,s_k}$ is given by

$$\mu(h_{s_0,\ldots,s_k}) = a_{s_0} \prod_{i=1}^{k} W_1(s_i, s_{i-1}).$$

The area of all the strips produced by iterating h_1 k times is given by

$$\mu\left(F^k h_1 \cap S\right) = |(a_1, 0) \cdot W_1^k|.$$

Therefore, the portion of h_1 which escapes at the kth iterate can be approximated by

$$\mathrm{esc}_k(h_1) = \mu\left(F^{k-1} h_1 \cap S\right) - \mu\left(F^k h_1 \cap S\right) = |(a_1, 0) \cdot W_1^{k-1}(I - W_1)|$$

and a similar expression can be written for h_2. Since the only mechanism for escape from S is through the lobe D_0, we obtain $\mathrm{esc}_k(h_1) = \mu(F^k h_1 \cap D_0)$. Hence, given the areas a_1 and a_2 of the horizontal strips of $E_{n_0} \cap S$ which lie in H_1 and H_2, respectively, we use the above equations to find the $e_n \equiv \mu(E_n \cap D_0)$ for $n > n_0$:

$$e_n = |(a_1, a_2)\left(W_1^{n-1-n_0} - W_1^{n-n_0}\right)| = |(a_1, a_2) W_1^{n-n_0-1}(I - W_1)|. \tag{7}$$

Finding the e_n for $n < n_0$ can be done numerically, or via a Whisker map approximation as derived in section 9.

In RLW and RW it was shown that one can compute all the relevant transport quantities using the e_n's; for example, the amount of phase space area originating in $\hat{S}$ which escapes at the nth iteration, c_n, and the amount of phase space area originating in $\hat{S}$ which stays in $\hat{S}$ after the nth iteration, R_n, are given by

$$\begin{aligned} c_n &= \mu\left(F^n(\hat{S}) \cap D_0\right) = \mu(D_0) - \sum_{j=1}^{n-1} e_j, \\ R_n &= \mu\left(F^n(\hat{S}) \cap \hat{S}\right) = \mu(\hat{S}) - \sum_{j=1}^{n} c_j. \end{aligned} \tag{8}$$

In RLW the e_n's were computed numerically. The main result of this paper is the derivation of an analytical method for estimating the e_n's for all finite n and estimating their asymptotic behavior for large n. Computing these quantities was the major obstacle for applying the above formulae to a variety of flows and maps which arise in studying transport of passive scalars in fluids, transition probabilities in mechanics, reaction rates in chemistry and numerous other applications. Moreover, while for the two-dimensional case the computational approach is feasible, it is clearly a barrier for applications in higher dimensions. The ideas presented here carry over to higher dimensions in the same fashion as presented in ref. [11], and will be discussed in a subsequent paper.

3.3. *The stretching rates*

The distribution of the averaged stretching rates, measuring the averaged amount of stretching of a material line during its evolution through the region S (the average is over initial conditions, see RLW for more details), can be calculated as follows. The segments of K_0 which escape after n iterations are given by the horizontal boundaries of $D_{-n} \cap S$, namely $D_{-n} \cap K_0$, hence their length is given by the sum of the widths of the vertical strips:

$$L(D_{-n} \cap K_0) \approx |(\hat{w}_1, \hat{w}_2) \hat{W}_1^{(n-n_1)}|, \tag{9}$$

where $\hat{w}_1, \hat{w}_2$ are the widths of the vertical strips V_1, V_2 of $D_{-n_1} \cap S$ and $\hat{W}_1$ is the weighted transition matrix of the inverse map. The averaged stretching experienced by the segments of K_0 which escape after n iterations is given by

$$\beta(n) = \frac{L(K_n \cap D_0)}{L(K_0 \cap D_{-n})} \approx \frac{L(K_n \cap D_0)}{|(\hat{w}_1, \hat{w}_2)\hat{W}_1^{(n-n_1)}|}, \quad n_1 \leq n \tag{10}$$

and is bounded from above and below by

$$\frac{\frac{1}{2}r(0,n)\, L(K_1 \cap D_0)}{|(\hat{w}_1, \hat{w}_2)\hat{W}_1^{(n-n_1)}|} < \beta(n) < \frac{\frac{1}{2}r(0,n)\, L(K_0')}{|(\hat{w}_1, \hat{w}_2)\hat{W}_1^{(n-n_1)}|}, \quad n_1 \leq n. \tag{11}$$

For example, if $\hat{W}_1(i,j) = \frac{1}{3}$, $i,j = 1,2$ and $n_1 = 0$, eqs. (6), (11) imply that

$$\log 3 + \frac{\log L(K_1 \cap D_0)}{n} < \frac{\log \beta(n)}{n} < \log 3 + \frac{\log L(K_0')}{n}$$

and the length of the intervals which escape after n iterates, $L(K_0 \cap D_{-n})$, is given by $\frac{1}{2}(2/3)^n$. If one plotted $\beta(n)$ versus x, the position along K_0, a fractal function would emerge. The maximal stretching rate, which involves maximization over the initial direction of the line elements is bounded from below by eq. (11). However, using the same argument as for the topological entropy, it seems that the stretching rates measured along the manifold maximize $\beta(n)$ and hence that both bounds in (11) hold for the maximal stretching rate.

3.4. Type-l trellis

The generalization to the type-l case can be viewed in two equivalent manners; one is to note that the type-l trellis is basically a horseshoe map with a delay, namely if one defines horizontal strips as before, and the regions H_1 and H_{l+1} are chosen appropriately then one obtains the following diagram:

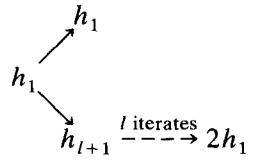

(12)

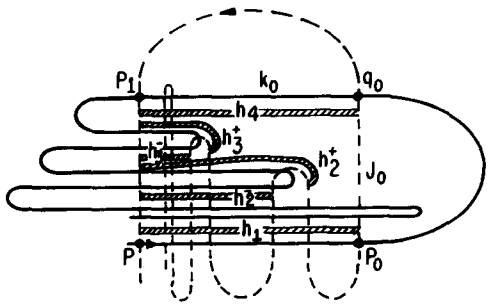

Fig. 4. The definition of states of a type-l trellis. In this figure $l = 3$.

hence one can introduce $2(l-1)$ fictitious states $H_2^{\pm},\ldots,H_{l-1}^{\pm}$ resulting in the following diagram:

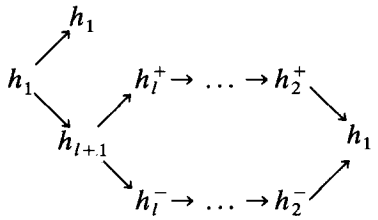

(13)

Equivalently one can define the regions explicitly as follows:

Let $y_j^{\pm}(t)$, $0 \le t \le 1$ and $1 \le j \le l+1$ denote "horizontal curves" in S such that

(i) The boundaries of the curves are given by

$$
\begin{aligned}
&y_1^+(0) \in J_j \cup J_j', && y_1^+(1) \in J_0, && j \ge l,\\
&y_j^+(0) \in J_{l-j+1}, && y_j^+(1) \in J_{-j+1}, && 1 < j \le l,\\
&y_j^-(0) \in J_{l-j+2} \cup J_{l-j+1}', && y_j^-(1) \in J_{-j+1}, && 1 < j \le l,\\
&y_{l+1}^-(0) \in J_1, && y_{l+1}^-(1) \in J_0.
\end{aligned}
$$

(ii) $y_j^{\pm}(t) \cap J_{-k}$, $0 < t < 1$ contains exactly two points if $\min\{j,l\} \le k \le l$ and is empty if $0 \le k < \min\{j,l\}$ for all $1 \le j \le l+1$.

A strip will be called horizontal of type h_j^+ (h_j^-) if it is topologically a rectangle and two of its edges are given by horizontal curves of type $y_j^+(t)$ ($y_j^-(t)$) and segments of J_{l-j+1} and J_{-j+1} (J_{l-j+2} and J_{-j+1}), see fig. 4.

Diagram (13) reflects the dynamics of the map on all the horizontal strips which are defined above where $h_1^+ \equiv h_1$ and $h_{l+1}^- \equiv h_{l+1}$. Similarly, one can define vertical strips of type $v_j^{\pm}$ and plot exactly the same diagram as in (13), replacing the h's with v's, which then reflects the action of the inverse map on all vertical strips. This definition of horizontal and vertical strips does not necessarily include all points in the region S. We choose this formulation since it leads to the simplest symbolic dynamics representation of the dynamics of the horizontal strips of $E_n \cap S$ under forward iterations (respectively, the dynamics of the vertical strips of $D_{-n} \cap S$ under backward iterations). The labels of the horizontal strips composing the set $E_n \cap S$ are one-sided symbol sequences of length n, and diagram (13) supplies the rules for obtaining the labels of the strips composing $E_{n+1} \cap S$ from the n-symbol sequences. The disadvantage of this choice of symbols is that it is not obvious how to create a bi-infinite sequence of symbols which under the shift map will be topologically conjugate to the dynamics of the map on the invariant set. Such a construction is necessary for obtaining information regarding the dynamics on the invariant set such as the number of periodic orbits of period $k \in \mathbb{Z}^+$. We note that other information, such as the area of the invariant set, can be inferred from the dynamics on the escaping portion, as shown in section 8.

At this point the analogy to the type-1 case is almost straightforward. We define the transition matrix and the weighted transition matrix T_l and W_l and compute all the topological and metric quantities which were defined for the type-1 case. The metric approximation involved in using W_l instead of the exact map for evaluating the transport rates is basically a semi-linear one, which seems dubious at first sight since for $l > 1$ the nature of the trellis inside S is highly nonlinear. However, since we let the curved

states h_i be stretched along the whole region before we again linearly approximate their partition, I believe the linear computation will give a good approximation to the escape rates and stretching spectra.

The general transition matrix T_l' resulting from diagram (13) is a $2l \times 2l$ matrix of the form

$$T_l' = \begin{array}{c} \\ h_1 \\ h_2^+ \\ h_2^- \\ h_3^+ \\ h_3^- \\ \vdots \\ h_{l+1} \end{array} \begin{array}{c} \begin{array}{ccccccc} h_1 & h_2^+ & h_2^- & \dots & h_l^+ & h_l^- & h_{l+1} \end{array} \\ \begin{pmatrix} 1 & 0 & 0 & \dots & 0 & 0 & 1 \\ 1 & 0 & 0 & \dots & 0 & 0 & 0 \\ 1 & 0 & 0 & \dots & 0 & 0 & 0 \\ 0 & 1 & 0 & \dots & 0 & 0 & 0 \\ 0 & 0 & 1 & \dots & 0 & 0 & 0 \\ \vdots & \vdots & \vdots & \ddots & \vdots & \vdots & \vdots \\ 0 & 0 & 0 & \dots & 1 & 1 & 0 \end{pmatrix} \end{array},$$

one can equivalently identify the states $h_i^{\pm}$ to one state h_i to obtain an $(l+1)\times(l+1)$ nonsingular transition matrix T_l of the form

$$T_l = \begin{pmatrix} 1 & 0 & 0 & \dots & 0 & 0 & 1 \\ 1 & 0 & 0 & \dots & 0 & 0 & 0 \\ 0 & 1 & 0 & \dots & 0 & 0 & 0 \\ 0 & 0 & 1 & \dots & 0 & 0 & 0 \\ \vdots & \vdots & \vdots & \ddots & \vdots & \vdots & \vdots \\ 0 & 0 & 0 & \dots & 1 & 0 & 0 \\ 0 & 0 & 0 & \dots & 0 & 2 & 0 \end{pmatrix}.$$

The reason for introducing the extended matrix and the states $h_i^{\pm}$ initially is that they are essential for broadening the class of trellises as shown in the next section.

The consequences of diagram (13) and the form of the transition matrix are as follows:

(a) Number of horizontal strips in h_i after n iterations: given the $(l+1)$-dimensional vector v^0 of initial number of strips in the regions h_i, the number of strips in each region after the nth iteration is given by v^n:

$$v^n = v^0 \cdot T_l^n. \tag{14}$$

In other words, since there is a one-to-one correspondence between labeling of horizontal strips and the allowed sequences of the $l+1$ symbols, one gets that the number of strips is amplified exactly as the number of allowed sequences.

The number of strips of $E_n \cap S$ of type h_j is obtained by taking $v^1 = (0,\dots,0,1,0)$, hence is given by the lth row of T_l^{n-1}. Denoting the ith row of T_l by $T_l(i)$, and using the form of T_l, we obtain

$$\begin{aligned} &T_l^n(1) = T_l^{n-1}(1) + T_l^{n-1}(l+1) = T_l(1) + \sum_{j=1}^{n-1} T_l^j(l+1), && n > 1, \\ &T_l^n(l+1) = 2T_l^{n-1}(l) = 2T_l(1-n+2), && n \le l+1, \\ &T_l^n(l+1) = 2T_l^{n-l}(1), && n > l+1, \end{aligned} \tag{15}$$

hence we obtain the following recursion relations for the $(l+1)$th row of T_l:

$$\begin{aligned} T_l^n(l+1) &= 2T_l(l-n+2), && n \le l+1, \\ T_l^n(l+1) &= 2\left(T_l(1) + \sum_{j=1}^{n-l-1} T_l^j(l+1)\right), && n > l+1, \end{aligned} \tag{16}$$

which results in the following simple equation for the $(l+1)$th row:

$$\begin{aligned} T_l^n(l+1) &= 2T_l(l-n+2), && n \le l+1, \\ T_l^{l+2}(l+1) &= 2T_l(1) + T_l(l+1), \\ T_l^n(l+1) &= T_l^{n-1}(l+1) + T_l^{n-l-1}(l+1), && n > l+2 \end{aligned} \tag{17}$$

and the other rows are given by

$$\begin{aligned} T_l^n(1) &= T_l(1) + \sum_{j=1}^{n-1} T_l^j(l+1), && n > 1, \\ T_l^n(j) &= T_l^{n-1}(j-1), && 1 < j \le l, \quad n > 1, \end{aligned} \tag{18}$$

hence

$$v^n = T_l^{n-1}(l) = T_l^n(l+1), \quad n > 1 \tag{19}$$

and eq. (18) supplies a recursion relation for v^n.

(b) Number of points in $J_0 \cap K_n$, $r(0,n)$: using eq. (14), the observation that the only horizontal strips which intersect J_0 are h_1 and h_{l+1}, intersecting J_0 at exactly two points, and that K_{l+1} contains exactly two horizontal strips $h_1 \cup h_{l+1}$, we obtain

$$\begin{aligned} r(0,n) &= 0, && 1 \le n \le l-1, \\ r(0,l) &= 2, \\ r(0,n) &= (2,0,\ldots,0,2)T_l^{n-l-1}(1,0,\ldots,0,1)^{\mathrm{T}}, && l+1 \le n, \end{aligned}$$

using (15) and the form of T_l we obtain

$$\begin{aligned} r(0,0) &= 1, \\ r(0,n) &= 0, && 1 \le n \le l-1 \\ r(0,l) &= 2, \\ r(0,n+1) &= r(0,n) + 2r(0,n-l), && l \le n, \end{aligned} \tag{20}$$

which agrees with Judd's [13] result and differs from Easton's by one index.

(c) The topological entropy, defined as the exponential growth rate of $L(K_n)$, is equal to the exponential growth rate of the number of strips created by E_n. From eq. (19) it is given by $\alpha = \lim_{n\to\infty} n^{-1} \log|T_l^n(l+1)|$. Since the roots of the characteristic polynomial of T_l, $p_{T_l}(\lambda) = \lambda^{l+1} - \lambda^l - 2$, are distinct, the topological entropy is given by the root with the largest modulus, λ_l. For large l the

moduli of the roots of p_{T_l} are clustered in the interval $[1, \lambda_l]$, where $\lambda_l \to 1$ as $l \to \infty$. Hence, as l increases the transient time before the exponential behavior of the growth rate can be detected, gets longer, and in the limit of infinite l nonexponential behavior is expected. As discussed by MacKay et al. [4], these are delicate points when one analyses the long-time behavior. The topological entropy provides a first estimate to the length of the boundary of E_n, hence to the length of the development of $W^u_+, L(W^u_{+,n})$, but we defer the discussion of the exact form of these estimates to section 6.

3.5. *Escape rates for the type-l trellises*

To obtain metric properties such as the escape rates and the distribution of the Lyapunov exponents on K_0, we assign weights to the transition matrix T_l which are determined by the metric properties of the initial development of the trellis. Let W_l' and W_l be the extended and regular weighted matrices. These matrices are determined by the four terms $W_l'(1,1), W_l'(1,2l), W_l'(2l, 2l-2), W_l'(2l, 2l-1)$ (denoted hereafter by s_1, s_2, s_3, s_4, respectively) which are associated with the amount of stretching experienced by segments of strips h_1 and h_{l+1} as shown in fig. 2. The matrices W_l', W_l are of the form

$$W_l' = \begin{array}{c} \\ h_1 \\ h_2^+ \\ h_2^- \\ h_3^+ \\ h_3^- \\ \vdots \\ h_{l+1} \end{array} \begin{array}{c} \begin{array}{ccccccc} h_1 & h_2^+ & h_2^- & \dots & h_l^+ & h_l^- & h_{l+1} \end{array} \\ \begin{pmatrix} s_1 & 0 & 0 & \dots & 0 & 0 & s_2 \\ 1 & 0 & 0 & \dots & 0 & 0 & 0 \\ 1 & 0 & 0 & \dots & 0 & 0 & 0 \\ 0 & 1 & 0 & \dots & 0 & 0 & 0 \\ 0 & 0 & 1 & \dots & 0 & 0 & 0 \\ \vdots & \vdots & \vdots & \ddots & \vdots & \vdots & \vdots \\ 0 & 0 & 0 & \dots & s_3 & s_4 & 0 \end{pmatrix} \end{array}$$

and

$$W_l = \begin{pmatrix} s_1 & 0 & 0 & \dots & 0 & 0 & s_2 \\ 1 & 0 & 0 & \dots & 0 & 0 & 0 \\ 0 & 1 & 0 & \dots & 0 & 0 & 0 \\ 0 & 0 & 1 & \dots & 0 & 0 & 0 \\ \vdots & \vdots & \vdots & \ddots & \vdots & \vdots & \vdots \\ 0 & 0 & 0 & \dots & 1 & 0 & 0 \\ 0 & 0 & 0 & \dots & 0 & s_3 + s_4 & 0 \end{pmatrix}.$$

The assumption that the trellis satisfies hypothesis C is used to establish that the only stages at which area is thrown out are when h_1 is mapped to $h_1 \cup h_{l+1}$ and the lth image of the mapping of h_{l+1} to $h_l^{\pm}$. The weighted transition matrix provides the area of the strip $h_{s_0,\dots,s_k}$ since

$$\mu(h_{s_0,\dots,s_k}) = a_{s_0} \prod_{i=1}^{k} W_l(s_i, s_{i-1}),$$

where a_{s_0} is the area of the strip h_{s_0}. Hence, the area of all the strips produced by iterating h_1 k times is given by $|(a_1, 0, \dots, 0) \cdot W_l^k|$. Unlike the situation in the $l = 1$ case, this quantity is not equal to $\mu(F^k h_1 \cap S)$: we have thrown away the parts of $F^k h_1$ which are yet to escape S between the $k+1$ and

the $k+l$ iterations. There are two methods to overcome this difficulty; the first is to stretch back the central $l-1$ components of the vector $(a_1,0,\ldots,0)\cdot W_l^k$ by $1/(s_3+s_4)$ and the second is to add more intermediate states which contain the delayed escaping parts.

Using the first method, the portion of h_1 which escapes at the kth iterate can be approximated by

$$\mathrm{esc}_k(h_1)=\mu\big(F^{k-1}h_1\cap S\big)-\mu\big(F^k h_1\cap S\big)=|(a_1,0,\ldots,0)\cdot W_l^{k-1}(I-W_l)D|,$$

where D is the $(l+1)\times(l+1)$ diagonal matrix with the diagonal $(1,1/(s_3+s_4),\ldots,1/(s_3+s_4),1)$. Note that since the only mechanism for escape from S is through the lobe D_0, the relation $\mathrm{esc}_k(h_1)=\mu(F^k h_1\cap D_0)$ holds. Hence, assuming that E_l is already stretched enough for the linear approximation to hold, and that the area of $E_l\cap S$ is given by a_1, we find

$$e_n=|(a_1,0,\ldots,0)\cdot\big(W_l^{n-l-1}(I-W_l)D\big)|,\quad n>l. \tag{21}$$

Using eq. (8) one can therefore estimate all the escape rates needed.

To obtain the e_n's from a higher-order approximation where the area of the h_j's are given for $j\geq 1$ we need to use the second method, hence to introduce $l+1$ more states, denoted by g_j, $0\leq j\leq l$, which are basically the delayed escaping rates. These states are passive and do not influence the dynamics of the other states, and their introduction allows us, in addition to the computation of the escape rates, to draw the analog between the weighted transition matrix and the fundamental matrix of a finite Markov chain [21]. Moreover, the introduction of these states is essential for computing the escape rates in the next generalization of the type-l trellises to the type-$\{l,m,k,x\}$ trellises.

The intuitive definition of the states g_j is given below, where an exact definition, as was given for the h_j's is trivial and is left to the reader. In general, the state g_i contains the "excess" part of h_i which escapes after i iterations and therefore is not considered part of the h's. The state g_l is the part of the image of h_{l+1} which escapes after l iterations and is given by $[F(h_{l+1})-h_{l+1,l^+}-h_{l+1,1^-}]$. The next $l-1$ states are the images of g_l, namely $g_k=F(g_{k+1})$, $1<k<l$. The state g_1 is composed from the delayed escaping area, $F(g_2)=F^{l-1}(g_l)$, and the escaping part of h_1: $g_1=[F(h_1)-h_{1,1}-h_{1,l+1}]+F(g_2)$. Finally, g_0 is the total escape rate and is given by $g_0=\Sigma_{k>0}F^k(g_1)$. The state g_0 is introduced to make the analog to the Markov chain formalism immediate, and is dropped when appropriate (e.g. when computing the eigenvalues of the extended matrix).

The extended transition matrix, M, is given by:

$$M=\begin{array}{c} \begin{matrix} g_0\cdots g_l & h_1\cdots h_{l+1} \end{matrix} \\ \begin{pmatrix} L_{l+1} & 0 \\ R & W_l \end{pmatrix} \end{array}, \tag{22}$$

where L_n is an $n\times n$ matrix of the form

$$L_n=\begin{pmatrix} 1 & 0 & 0 & \ldots & 0 & 0 & 0 \\ 1 & 0 & 0 & \ldots & 0 & 0 & 0 \\ 0 & 1 & 0 & \ldots & 0 & 0 & 0 \\ 0 & 0 & 1 & \ldots & 0 & 0 & 0 \\ \vdots & \vdots & \vdots & \ddots & \vdots & \vdots & \vdots \\ 0 & 0 & 0 & \ldots & 1 & 0 & 0 \\ 0 & 0 & 0 & \ldots & 0 & 1 & 0 \end{pmatrix} \tag{23}$$

and R is given by

$$R(1,2) = 1 - s_1 - s_2, \quad R(l+1, l+1) = 1 - s_3 - s_4, \quad R(i,j) = 0 \quad \text{otherwise.}$$

Denoting by v^n the $(2l+2)$-dimensional vector which contains the area in each state $(g_0, \ldots, h_{l+1})$ of E_n, it is clear that the escape rates are given by the second component of v^n, $v^n(2)$:

$$e_n = (v^{n_0} \cdot M^{n-n_0})(2), \quad n > n_0.$$

Finding the e_n for $n < n_0$ can be done numerically, or via a Whisker map approximation as derived in section 9. For $n \gg n_0$, the asymptotic behavior of the e_n's depends on the nature of the eigenvalues and eigenvectors of the matrix M. Since the characteristic polynomial of W and M are given by

$$P_W(\lambda) = (\lambda - s_1)\lambda^l - s_2(s_3 + s_4),$$

$$P_M(\lambda) = P_W(\lambda)(\lambda - 1)\lambda^l$$

it is sufficient to examine W. P_W has $l+1$ distinct roots, hence the e_n's decay exponentially with the decay rate $\log(\lambda_{W_l})$. As is the case for the topological entropy, one finds that the roots moduli of P_{W_l} cluster in an interval $[|\lambda_{\bar{W}_l}|, |\lambda_{W_l}|]$ (with $|\lambda_{W_l}| < 1$) and both end points approach one asymptotically as l increases. Hence, the decay rate will appear to be different than exponential for longer and longer time as l is increased, and in the infinite l limit a nonexponential decay rate of the e_n's will emerge.

Note that eq. (22) shows that the dynamics of the strips can be thought of as a Markov chain where the probabilities correspond to area distribution, the states $g_0, \ldots, g_l$ are an absorbing chain, and the states $h_0, \ldots, h_{l+1}$ are transient states. The matrix M is in its canonical form [21] and hence one can compute various quantities associated with this formulation as discussed in section 8.

3.6. *The stretching rates for type-l trellises*

Following the same arguments as for the horseshoe trellis we find that the length of the horizontal boundaries of $D_{-n} \cap S$, namely $D_{-n} \cap K_0$, is given by the sum of the widths of the vertical strips of type v_1 and v_{l+1}, the only vertical strips which cut through K_0. Hence, given the areas $a_1, \ldots, a_{l+1}$ of the vertical strips $v_1, \ldots, v_{l+l}$, we obtain

$$L(D_{-n} \cap K_0) \approx \frac{1}{L(J_0)}(a_1, \ldots, a_l) \cdot \hat{W}_l^{(n-n_1)} \cdot (1, 0, \ldots, 0, 1)^{\mathrm{T}}, \tag{24}$$

where $\hat{W}_l$ is the weighted transition matrix of the inverse map. The averaged stretching experienced by the segments of K_0 which escape after n iterations is given by

$$\beta(n) = \frac{L(K_n \cap D_0)}{L(K_0 \cap D_{-n})} \tag{25}$$

and this quantity can be bounded from above and below as was done for the horseshoe to obtain

$$\frac{\frac{1}{2}r(0,n)\,L(K_1\cap D_0)}{L(D_{-n}\cap K_0)}<\beta(n)<\frac{\frac{1}{2}r(0,n)\,L(K_0')}{L(D_{-n}\cap K_0)},\quad n_1\le n. \tag{26}$$

As before, the dependence of $\beta(n)$ on position along K_0 is of fractal nature. Eq. (25) implies that the asymptotic behavior of $\beta(n)$ is given by

$$\lim_{n\to\infty}\frac{\log\beta(n)}{n}=\log\left(\frac{\lambda_T}{\lambda_{\hat{W}}}\right),$$

where λ_A denotes the largest eigenvalues of the matrix A.

4. Trellises of type $\{l, m, k, x\}$

In this section we construct a new class of trellises. This is done for two purposes; first, to show that one can improve the estimates for a given trellis in a consistent fashion by adding more symbols to the symbolic dynamics representation of the trellis, hence achieving better estimates on the transport rates and manifold length, and second, to show that if the initial developments of two trellises are sufficiently close the above characteristics of the trellises are also close. This will support the claim that a reasonable approximation is already given by considering an $\{l, m, k, x\}$ trellis rather than the most general trellis which is defined by infinitely many indices.

4.1. The definition of a type-{l, m, k, 0} trellis

To modify Easton's definition we keep his first two hypotheses and change the third one. Easton's third hypothesis implied that the "tip" of the lobe E_r had to be completely contained in the lobe D_{r-l}, and that no new "tips" could be created. We will modify the first part of the assumption but will stick to the second part of it.

We present the geometrical assumptions and the meaning of the indices l, m, k, x for the extended family of trellises. The formal definition for the $x=0$ case, and the proof that two type-$\{l, m, k, 0\}$ trellises are weakly equivalent and therefore are well defined is given in the appendix.

The geometrical assumptions are as follows, see fig. 5:

(1) l is defined to be the minimal j such that $K_j\cap J_0\neq\emptyset$. We assume that $K_l\cap J_0$ contains four homoclinic points with stable and unstable orderings as depicted in fig. 5.

(2) $m\ge l$ is defined so that the tip of the lobe E_r is contained in the lobe D_{r-l-m} for all r.

(3) $k\ge l$ is defined so that the tip of D_{-r} is contained in the lobe E_{k-r+l} for all r.

(4) There are exactly two tips for the E_r, D_r lobes for all r, where by "tip" we mean a two- (or three-) point intersection of the lobes.

(5) $x=0$ indicates the following three assumptions:

(i) The connected part of $K_l\cap S$ ($J_{-l}\cap S$) which contains the tip intersects D_{-m} (E_k) only at the tip.

(ii) All the segments of the unstable manifold encircling the tip of E_l are contained in D_{-m}.

(iii) None of the segments of the stable manifold encircling the tip of D_{-l} are contained in E_k.

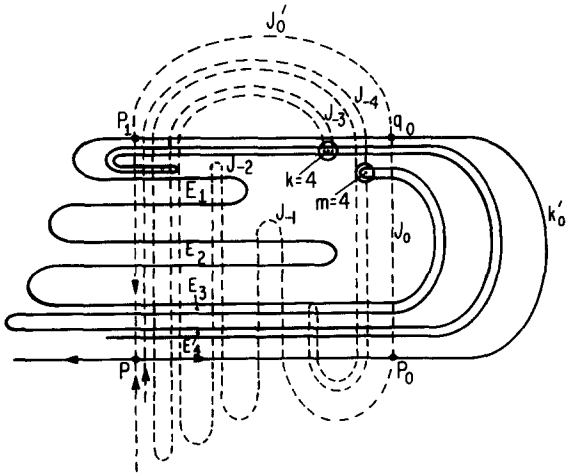

Fig. 5. The geometry of a type-$\{l, m, k, 0\}$ trellis. In this figure $l = 3$, $m = k = 4$.

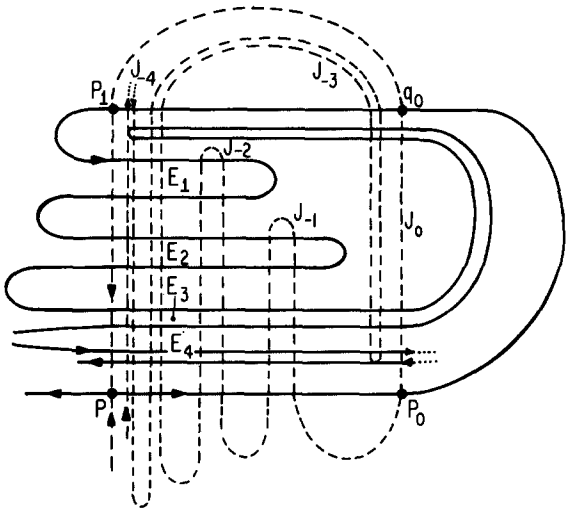

Fig. 6. The geometry of a type-$\{l + 1, m, k, -1\}$ trellis. In this figure $l = 3$, $m = k = 4$.

Few notes are now in order:

(a) The type-$\{l, m, k, 0\}$ trellis asymptote topologically to the type-l trellis as $m, k \to \infty$.

(b) It is more convenient to replace (5iii) by the assumption that the tip of D_{-l} is actually tangent to E_k, creating a three-point tip as shown in fig. 5, as we do in the formal definition.

(c) Assumption (5ii) can be rephrased as follows: All the segments of the unstable manifold encircling the tip of E_{l+m} are contained in D_0. This version demonstrates more clearly the equivalence between the above assumptions and Easton's construction of type-l trellises.

(d) Given Easton's work and the above generalization, other geometries can be handled similarly. We describe next a specific generalization, which is of importance since it is expected to appear in many applications, but as mentioned before the number of variations on the above assumptions is infinite.

4.2. Other trellises of type {l, m, k, x}

Other trellises of type $\{l, m, k, x\}$ correspond to various variation on the fifth structural assumption. For example, keeping assumption (5i) and interchanging assumptions (5ii) and (5iii) will result in three more trellises, $x = 1, 2, 3$, where dropping the requirement that either all or none of the encircling segments are contained in the corresponding lobe will introduce more indices corresponding to the next approximation to a "real" trellis. For each of these structures we can modify assumption (5i) to allow $4j + 2$ ($j \in \mathbb{Z}^+$) intersections of the connected part of $K_l \cap S$ or/and $J_{-l} \cap S$ with D_{-m} and E_k, resulting in $x \in \mathbb{Z}^+$. Of particular interest is the other extreme to the $x = 0$ case, where the connected part of $K_l \cap S$ almost reaches J_1, hence intersects the D_{-j} lobes the same way as K_0 does (though twice) for $1 < j < m$ and misses only the last intersection (in the unstable ordering) of $K_0 \cap D_{-m}$ as shown in fig. 6. For $x = 0$ the limit $m, k \to \infty$ corresponds to approaching the type-l trellis from above where in this case $m, k \to \infty$ corresponds to approaching the type-$(l + 1)$ trellis from below, hence the notation $\{l + 1, m, k, x\}$, where $x \in \mathbb{Z}^-$ can be introduced to label this extreme. Though the details in applying the following procedure for this case is different, the spirit is the same, and is left out of this paper.

Note that even though we allowed different developments than the ones considered by Easton, we still assume that a finite number of indices determine the intersection matrix $M(n,m)$, namely that no unconstrained intersections are allowed to occur. If a trellis has the same initial development as a type-$\{l,m,k,0\}$ trellis, the above rules give a lower bound on the terms of $r(n,m)$.

5. Symbolic dynamics for type-$\{l,m,k,0\}$ trellises

In this section we associate with every type-$\{l,m,k,0\}$ trellis symbolic dynamics and a transition matrix. This formulation allows one to compute the number of homoclinic points, the number of strips and to approximate the area ejected out every iteration, as well as topological properties such as the topological entropy.

We generalize the symbolic dynamics of the type-l case by introducing $l+m-1$ new horizontal strips, denoted by f_j, $-m+2 \le j \le l$, and additional $k-l+1$ intermediate horizontal strips, $h_{l+1}^{\pm}$ and h_j, $l-k+1 \le j \le 0$, see fig. 7. The horizontal strips are defined as follows:

Let $y_j^{\pm}(t)$, $0 \le t \le 1$, $-(k-l)-1 \le j \le l+1$, denote "horizontal curves" in S such that

(i) The boundaries of the curves are given by

$$
\begin{aligned}
&y_j(0) \in \bigcup_{k=0}^{\infty} J_{k+j} \cup J'_{k+j} && y_j(1) \in J_0, && j = l-k+1,\\
&y_j(0) \in J_{l-j+1} \cup J'_{l-j}, && y_j(1) \in J_0, && -(k-l)+2 \le j \le 1,\\
&y_j^+(0) \in J_{l-j+1}, && y_j^+(1) \in J_{-j+1} && 1 < j \le l,\\
&y_j^-(0) \in J_{l-j+2} \cup J'_{l-j+1}, && y_j^-(1) \in J_{-j+1}, && 1 < j \le l,\\
&y_{l+1}^{\pm}(0) \in J_1, && y_{l+1}^{\pm}(1) \in J_0.
\end{aligned}
$$

(ii) $y_j^{\pm}(t) \cap J_{-k}$, $0 < t < 1$ contains exactly two points if $\max\{-1, j\} \le k \le l$ and is empty if $0 \le k \le j-1$ for $-(k-l)-1 \le j \le l$.

(iii) $y_{l+1}^{\pm}(t) \cap J_{-k} = \emptyset$, $0 < t < 1$, $0 \le k < l$, $y_{l+1}^{-}(t) \cap J_{-l}$, $0 < t < 1$ contains exactly two points, and $y_{l+1}^{+}(t) \cap J_{-l}$, $0 < t < 1$ contains exactly two points on each of the two connected components of $D_{-l} \cap S$.

In addition, let $z_j(t)$, $0 \le t \le 1$, $-m+2 \le j \le l$ denote "horizontal curves" in S such that

(i) The boundaries of the curves are given by

$$z_j(0) \in J_{-j+1}, \qquad z_j(1) \in J_{-m-j+1}, \quad -m+2 \le j \le l.$$

(ii) $z_j(t) \cap J_{-k}$, $0 < t < 1$ contains exactly two points if $-j-m-l+1 < k < -j-m+1$ and is empty if $-j-m+1 \le k \le -j+1$.

A strip will be called horizontal of type h_j^+ (h_j^-) if it is topologically a rectangle and two of its edges are given by horizontal curves of type $y_j^+(t)$ ($y_j^-(t)$) and segments of J_{l-j+1} and J_{-j+1} (J_{l-j+2} and J_{-j+1}) for $l-k+1 < j < l+1$, where for $j \le 1$ we disregard the $+$ sign on the y's and h's. It will be

called horizontal of type h^+_{l+1} (h^-_{l+1}) if it is topologically a rectangle and two of its edges are given by horizontal curves of type $y^+_{l+1}(t)$ ($y^-_{l+1}(t)$) and segments of J_1 and J_0. It will be called horizontal of type f_j if it is topologically a rectangle and two of its edges are given by horizontal curves of type $z_j(t)$ and segments of J_{-j+1} and J_{-j-m+1}.

Using the above definition we obtain the following diagram, which describes the dynamics of these horizontal strips under the map:

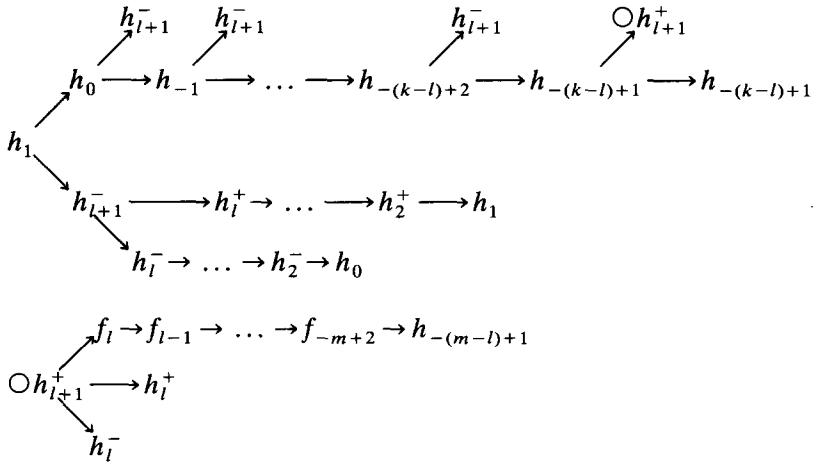

(27)

Given this diagram and the information that $E_1 \cap S$ is composed from an h^-_l strip and an f_l strip we construct the transition matrix, the weighted transition matrix and obtain all the quantities as before.

Note that when $m = l + 1$ the horizontal strips h^-_j and f_{j-m} can be identified for $2 \le j \le l$, reducing the number of required symbols by $m - 2 = l - 1$, see fig. 7.

Diagram (27) reflects the dynamics of the map on all the horizontal strips which are defined above. Similarly, one can define vertical strips of type $v^{\pm}_j$ and plot a diagram similar to (27), replacing the h's

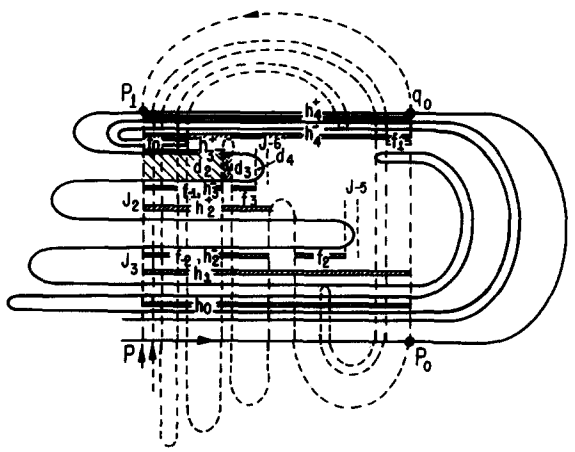

Fig. 7. The definition of the states of a type-$\{l, m, k, 0\}$ trellis. In this figure $l = 3$, $m = k = 4$.

with v's, which then reflects the action of the inverse map on all vertical strips which are defined in a similar fashion. The discussion of the relation between the dynamics of the map and the symbolic dynamics is as for the type-l trellis.

The general transition matrix $T_{l,m,k,0} \equiv T$ resulting from diagram (27) is a $(2l+k+m)\times(2l+k+m)$ matrix of the form

$$T = \begin{array}{c} \begin{matrix} h_{l-k+1}\dots h_1 & h_2^- \dots h_l^+ & h_{l+1}^- h_{l+1}^+ & f_{-m+2}\dots f_l \end{matrix} \\ \begin{pmatrix} L_{k-l+1} & 0 & A & 0 \\ \delta_{1,k-1}+\delta_{2,k-l+1} & L'_{2l-2} & 0 & 0 \\ 0 & B & 0 & 2\delta_{2,l+m-1} \\ \delta_{1,\max\{1,k-m+1\}} & 0 & 0 & L_{l+m-1}-\delta_{1,1} \end{pmatrix} \end{array},$$

where the states are ordered as follows:

$$\{h_{l-k+1}, h_{l-k+2}, \dots, h_{-1}, h_0, h_1, h_2^-, h_2^+, \dots, h_l^-, h_l^+, h_{l+1}^-, h_{l+1}^+, f_{-m+2}, \dots, f_l\}$$

and the matrices are defined as follows:

$\delta_{i,j}(i,j) = 1$ and all its other entries are zero.

L_n is an $n \times n$ matrix as in eq. (23).

L'_n is an $n \times n$ matrix with the nonvanishing terms $L'_n(i, i-2) = 1$ for $2 < i \le n$.

A is an $(k-l+1)\times 2$ of the form

$$A = \begin{pmatrix} 0 & 1 \\ 1 & 0 \\ \vdots & \vdots \\ 1 & 0 \end{pmatrix}.$$

B is an $2 \times (2l-2)$ matrix of the form

$$B = \begin{pmatrix} 0 & \dots & 0 & 1 & 1 \\ 0 & \dots & 0 & 1 & 1 \end{pmatrix}.$$

Using the same arguments as for the type-l trellis we obtain from T the following results:

(a) The number of strips in state i after n iterations is given by

$$v^n = v^0 \cdot T_l^n, \tag{28}$$

where v^0 represents the initial distribution of the strips between the states. The number of strips of $E_n \cap S$ of type j is obtained by taking $v^1(j) = 1$, $j = k+l-1, 2l+k+m$ and $v^1(j) = 0$ otherwise, hence is given by the sum of the $(k+l-1)$th and the last rows of T^{n-1}.

(b) Using eq. (28), the observation that the horizontal strips which intersect J_0 are h_j, $l-k+1 \le j \le 1$, $h_{l+1}^{\pm}$ and f_1, each of them intersecting J_0 at exactly two points, and that K_1 contains exactly two

horizontal strips $h_l^- \cup f_l$, we obtain the number of points in $J_0 \cap K_n$, $r(0,n)$:

$$\begin{aligned} r(0,n) &= (0,\dots,0,1,0,\dots,0,1)T^{n-1}(2,\dots,2,0,\dots,0,2,2,0,\dots,0,2,0,\dots,0) \\ &= 2\Bigg(\sum_{j=1}^{k-l+1} \left[T^{n-1}(k+l-1,j) + T^{n-1}(2l+k+m,j)\right] \\ &\quad + \sum_{j=k+l}^{k+l+1} \left[T^{n-1}(k+l-1,j) + T^{n-1}(2l+k+m,j)\right] \\ &\quad + \left[T^{n-1}(k+l-1,l+m+k+1) + T^{n-1}(2l+k+m,l+m+k+1)\right]\Bigg). \end{aligned} \tag{29}$$

(c) The topological entropy is given by

$$\alpha = \lim_{n\to\infty} n^{-1}\log\left(|T^{n-1}(k+l-1)| + |T^{n-1}(2l+k+m)|\right)$$

and the asymptotic behavior of $|T^n(j)|$ depends on the eigenvalues of T.

5.1. *Escape rates for the type-{l, m, k, 0} trellises*

To obtain metric properties such as the escape rates and distribution of the stretching rates on K_0, we assign weights to the transition matrix T which will be determined by the metric properties of the initial development of the trellis. Then we add additional $l+m+1$ passive states $g_0,\dots,g_{l+m}$, which are used to find the escape rates. Let W be the weighted transition matrix. It is determined by seven terms denoted by s_i, $i=1,\dots,7$ which are associated with the amount of stretching experienced by segments of h_1 and $h_{l+1}^{\pm}$ strips as shown in fig. 8. The matrix W is of the form

$$W = \begin{pmatrix} s_1 \cdot L_{k-l+1} & 0 & s_2 \cdot A & 0 \\ \delta_{1,k-l} + \delta_{2,k-l+1} & L'_{2l-2} & 0 & 0 \\ 0 & C & 0 & s_6 \cdot \delta_{2,l+m-1} \\ \delta_{1,\max\{1,k-m+1\}} & 0 & 0 & L_{l+m-1} - \delta_{1,1} \end{pmatrix},$$

where C is an $2 \times (2l-2)$ matrix of the form

$$C = \begin{pmatrix} 0 & \dots & 0 & s_4 & s_3 \\ 0 & \dots & 0 & s_4 & s_5 \end{pmatrix}.$$

Adding the additional $l+m+1$ states g_j, $0 \le j \le l+m$, which are defined in the same fashion as in the type-l case we obtain the $(3l+2m+k+1) \times (3l+2m+k+1)$ extended transition matrix, M:

$$M = \begin{array}{c} g_0 \cdots g_{l+m} \quad h_{l-k+1} \cdots f_l \\ \begin{pmatrix} L_{l+m+1} & 0 \\ R & W \end{pmatrix} \end{array},$$

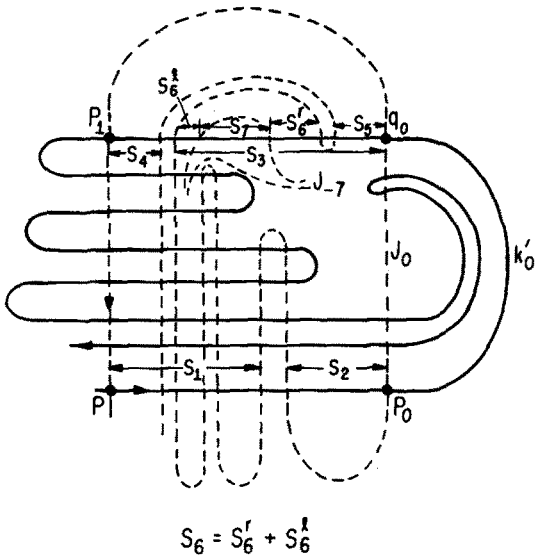

Fig. 8. The stretching rates of a type-$\{l, m, k, 0\}$ trellis. In this figure $l = 3$, $m = k = 4$. In addition to J_{-1}, J_{-2}, J_{-3} a part of J_{-7} is drawn.

where R is a $(2+m+k)\times(l+m+1)$ matrix which has the following non-vanishing entries:

$$R(j,2) = 1 - s_1 - s_2, \quad j = 1,\ldots,l+k-1,$$
$$R(k+l, l+1) = 1 - s_3 - s_4,$$
$$R(k+l+1, l+1) = 1 - \sum_{i=4}^{7} s_i,$$
$$R(k+l+1, l+m+1) = s_7,$$

corresponding to the escaping parts of the h_j's ($j \le 1$), of the h_{l+1}^- and h_{l+1}^+, respectively. Given this matrix, and following the same arguments as for the type-l trellis, we find that the escape rates can be approximated by

$$e_n = [(a_1,\ldots,a_{3l+2m+k+1})M^{n-n_0}](2), \tag{30}$$

where the a_j's denote the area distribution of E_{n_0} among the states. If $n_0 = 1$, the nonvanishing components of a are $(a_{l+1}, a_{l+m+1}, a_{2l+m+k-1}, a_{3l+2m+k-1})$ corresponding to the initial area in the states $(g_l, g_{l+m}, h_l^-, f_l)$ which are denoted by (d_1, d_4, d_2, d_3) in fig. 7. Note that the behavior of the e_n's for large n depends on the nature of the eigenvalues of W, as discussed previously. In section 9 we compute the e_n's for various l, m, k values and discuss their asymptotic behavior as m, k are increased.

5.2. *The stretching rates for type-{l, m, k, 0} trellises*

In this case the exact length of the horizontal boundaries of $D_{-n} \cap S$, namely $D_{-n} \cap K_0$, is harder to compute. In principal it is given by the sum of the widths of the vertical strips of type v_j, $j \le 1$ of the strips $v_{l+1}^{\pm}$ and the strip u_1, the vertical strips which cut through K_0. The width of the v_j's and v_{l+1}'s is

well approximated by taking their areas and dividing by $L(J_0)$. The width of u_1 can be approximated by either the width of v_1 or its area divided by the length of the tip of D_{-l}; however, this will be a poor approximation for the first few iterates, hence n_0 should be taken large enough, and in any case larger than $2l+m+k$. Using these approximations one can follow the same procedure as for the type-l trellises to compute the averaged stretching rates, etc.

6. The length of the unstable manifold

Since in many applications the length of the interface is of great importance, we devote this section to give various estimates for the length of the development of the unstable manifold. For example, the amount of product resulting from the mixing of two reacting fluids is related directly to the length of the interface between the two reactants, see ref. [22] and references therein. The relation between the stretching of a general material line and the unstable manifold was not established rigourously, though in RLW it was argued that in many cases the stretching of the interface will be almost the same as that of the unstable manifold.

Our aim is to get as sharp estimates as possible for the finite time development of the manifold. We concentrate on the finite time development for two reasons:

(1) The infinite time limit was already calculated in terms of the topological entropy (and was calculated for more general topology using similar ideas by Judd [13]).

(2) In many applications, especially in mixing problems, the finite-time behavior is more important than the asymptotics [23].

As noted in the first section, the unstable manifold is given by

$$W_+^u = \bigcup_{n=-\infty}^{\infty} K_n \cup K_n'.$$

Hence, the length of the development of the unstable manifold is given by

$$L_k = \sum_{n=-\infty}^{k} L(K_n) + L(K_n') = L_{k-1} + L(K_k) + L(K_k').$$

We assume that there exists a finite and sufficiently large n_0 ($n_0 > 0$) for which $L(K_j)$ and $L(K_j')$, $j \le n_0$, can be found either numerically or via a perturbation method.

By the assumption on the structure of the map (hypothesis B), the arcs K_n' are stretched only by the action of the fixed point, hence their length grows linearly for $n > n_0$, which from now on will be taken to be 1:

$$L(K_n') = L(K_{n-1}') + c_1 = (n-1)c_1 + L(K_1'). \tag{31}$$

To approximate $L(K_n)$ we decompose K_n to its components in S and the D lobes:

$$L(K_n) = L(K_n \cap S) + \sum_{j=0}^{n} L(K_n \cap D_j). \tag{32}$$

First, we will give bounds for the above quantities for the type-1 trellis for which

$$L(K_n \cap S) \approx r(0,n)\, L(K_0). \tag{33}$$

To bound the second term in (32), denote $c_2 = L(K_1 \cap D_0)$ and observe that

$$\begin{aligned} &\tfrac{1}{2}c_2 r(0,n) < L(K_n \cap D_0) < \tfrac{1}{2}L(K_0')\, r(0,n), \\ &\tfrac{1}{2}r(0,n-j)\,[c_2 + (j-1)c_1] < L(K_n \cap D_j) < \tfrac{1}{2}r(0,n-j)\, L(K_j'), \quad j > 0. \end{aligned} \tag{34}$$

Substituting (6), (31), (33) and (34) into (32), and assuming $L(K_0') = L(K_1')$ for simplicity, we obtain

$$\begin{aligned} &2^n\big[L(K_0) + c_2 - \tfrac{1}{4}c_1\big] - c_2 - (n - \tfrac{3}{2})c_1 < L(K_n) \\ &\quad < 2^n\big[L(K_0) + L(K_0') - \tfrac{1}{4}c_1\big] - L(K_0') - (n - \tfrac{3}{2})c_1. \end{aligned}$$

For a general type-$\{l,m,k,0\}$ or a type-l trellis, the only modification is that eq. (33) should be replaced by an inequality, bounding the length of the various strips from above and below. The upper bound for all the strips can be taken to be $L(K_0)$, where the lower bound is given in terms of the length of E_j, $j = 1,\ldots,l$, denoted by the vector Λ:

$$2v^n \cdot \Lambda < L(K_n \cap S) < 2|v^n| L(K_0), \tag{35}$$

where the number of strips of type h_i, f_i is given by v^n. Using eqs. (19), (20), (31), (32), (34) and (35) one obtains bounds on $L(K_n)$ for these trellises. For a general trellis, only the lower bound hold. As Camassa has pointed out, when the boundaries of E_j are nonconvex, one has to define the "length of E_j", Λ, with some care.

7. The relation between the type-l and the type-$\{l,m,k,0\}$ trellises

For m,k sufficiently large, one expects that the quantitative characteristics of the type-$\{l,m,k,0\}$ trellis will approach asymptotically the ones of the type-l trellis. The formulation in terms of the transition matrices enables one to quantify this limit by investigating the asymptotics of matrices instead of maps. Using the transition matrices and the weighted transition matrices which were constructed in sections 3 and 5, we find:

(i) The topological entropy of the type-$\{l,m,k,0\}$ trellises, which are estimated by the largest eigenvalue of the transition matrix $T_{l,m,k}$, approach asymptotically that of a type-l trellis in an exponential rate. Specifically,

$$\lambda_{T_{l,m,k,0}} \approx \lambda_{T_l} + c_l \exp\big[-b_l(m+k)\big]$$

as illustrated for $l = 2,6$ and $l+1 \le m$, $k \le l+15$ in figs. 9a and 9b. Fitting the calculations for $l = 1,\ldots,10$ we find that $b_l \approx -0.251 \log l + 0.011l + 0.68$ as demonstrated in fig. 9c.

(ii) The asymptotic behavior of the escape rates depends on the parameters s_i and the initial behavior depends on the d_i's as well. From the definition of the stretching rates s_i and the type-$\{l,m,k,0\}$ trellis it follows that as $m \to \infty$ the stretching rates s_6, s_7 should vanish and $s_5 \to s_3$. Since the width of the

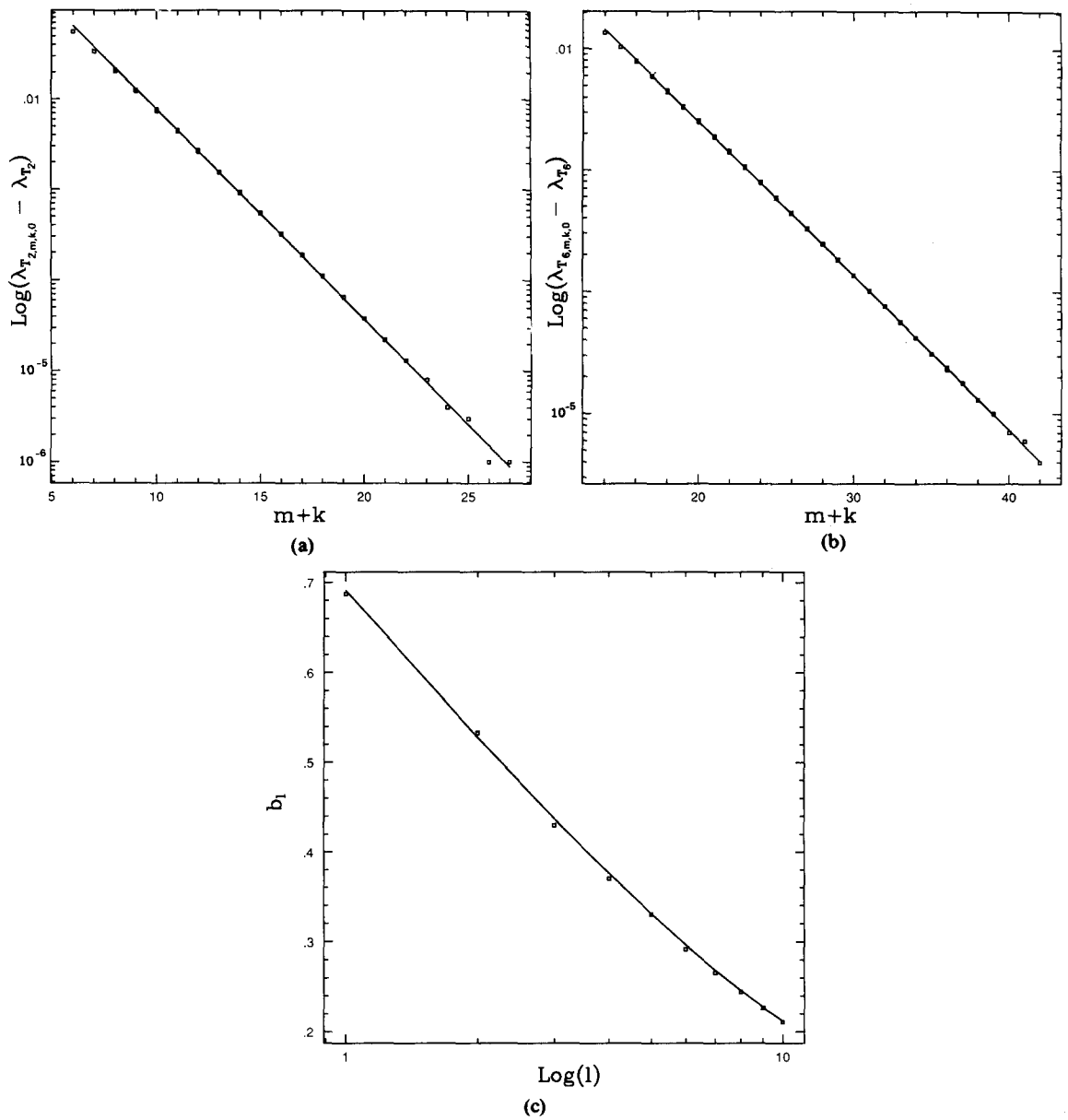

Fig. 9. Asymptotic behavior of the topological entropy for large m, k. (a) log–linear plot of $\lambda_{T_{2,m,k,0}} - \lambda_{T_2}$ versus $m+k$, $3 < m$, $k < 17$. (b) log–linear plot of $\lambda_{T_{6,m,k,0}} - \lambda_{T_6}$ versus $m+k$, $7 < m$, $k < 21$. (c) linear–log plot of b_l versus l, $1 < l < 10$, where b_l is the exponent found from the exponential relation demonstrated in (a) and (b). $3 < m$, $k < 17$.

rightmost vertical strip decays exponentially with the decay rate $\alpha = \log[L(J_0)/l_2]$, where l_2 denotes the vertical stretching rate as in fig. 8, we obtain that $s_7 = C_7 \exp(-\alpha m)$. Since the distance of the mth preimage of the unstable boundary of the lobe D from the fixed point is proportional to λ^{-m}, where λ is the largest eigenvalue of the fixed point, and by considering $F^{l+1}E$ and $F^{-m+1}D$ we obtain that $s_6 = C_6 \lambda^{-m}$. For simplicity we chose $\lambda = L(J_0)/l_2$ in the following computations, though in practice these rates vary with the parameters of the map and should be approximated via a calculation or a Whisker

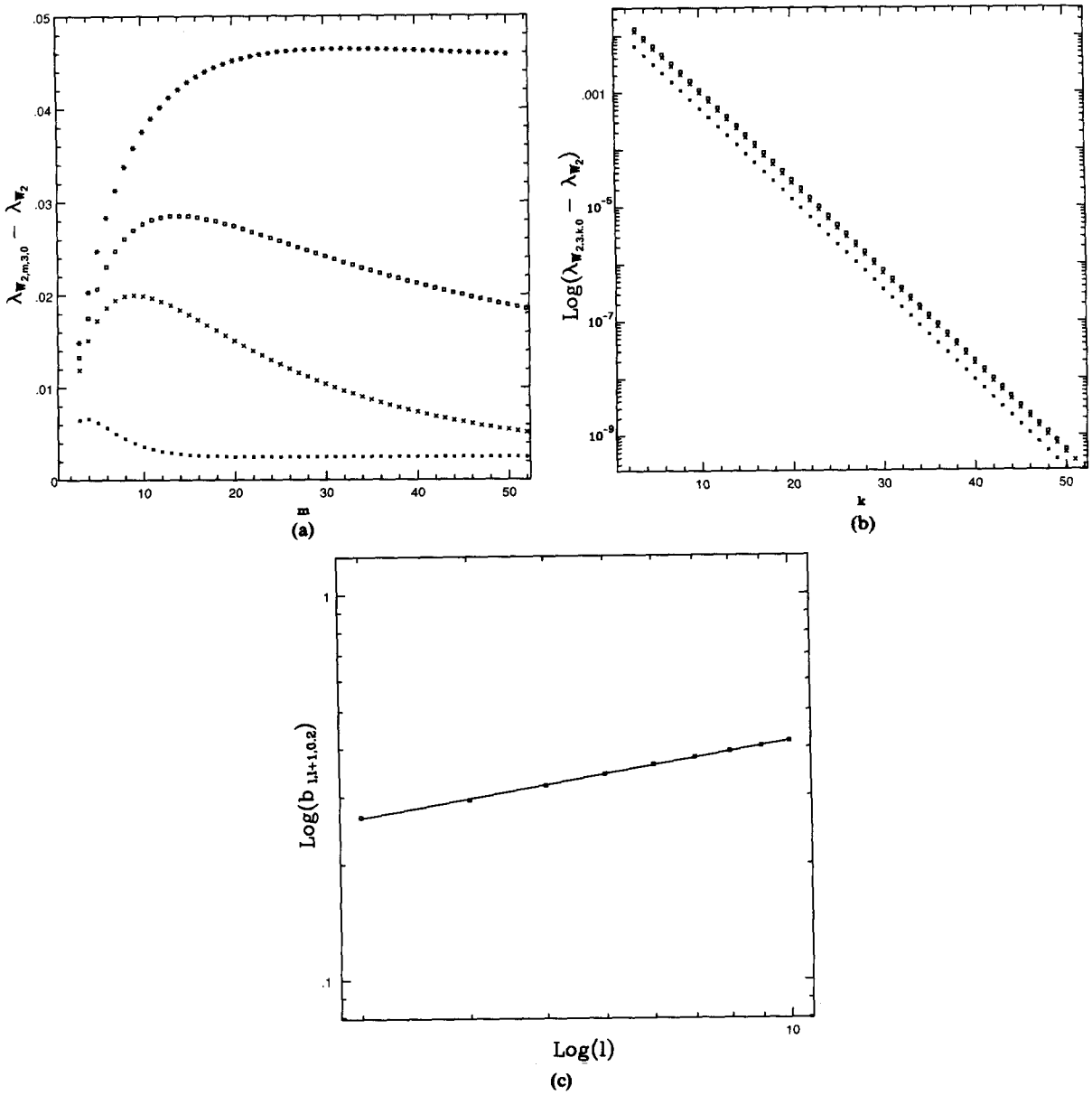

Fig. 10. Dependence of the asymptotic escape rate on l, m, k, α. (a) Plot of $\lambda_{W_{2,m,3,0}} - \lambda_{W_2}$ versus m, for four α values; (*) $\alpha = 0.1$, (□) $\alpha = 0.15$, (×) $\alpha = 0.2$, (■) $\alpha = 0.5$. (b) log–linear plot of $\lambda_{W_{2,3,k,0}} - \lambda_{W_2}$ versus k for various α values, denoted by the same symbols as in (a). This demonstrates the exponential behavior which determines $a_{l,m,\alpha}$ and $b_{l,m,\alpha}$. (c) log–log plot of the exponents $b_{l,m,\alpha}$ versus l, for $m = l + 1$ and $\alpha = 0.2$.

map approximation. With this choice of the s_i's we get

$$\lambda_{W_{l,m,k}} = \lambda_{W_l} + f(l,m,k,\alpha),$$

where $f(l,m,k,\alpha) \to 0$ as $m \to \infty$, or $k \to \infty$, but it is initially increasing with m as shown in fig. 10a for $l=2$, $k=3$ and several α values. For fixed m and α we obtain that

$$f(l,m,k,\alpha) \approx \exp(\alpha_{l,m,\alpha} - b_{l,m,\alpha} k)$$

and that the dependence of $b_{l,m,\alpha}$ on l is of a power law nature:

$$b_{l,m,\alpha} \approx c(m,\alpha)\, l^{d(m,\alpha)}$$

as shown in figs. 10b and 10c. The above relations are not exact, and we do find, for example, that $b_{l,m,\alpha}$ has a weak dependence on k. A proper analysis of these limits can be done by examining the characteristic polynomials of the matrices $W_{l,m,k}$. This is a very messy calculation which is under current investigation.

In fig. 11 we plot the escape rates for a type-5 and a type-$\{5,6,7,0\}$ trellis. The transient behavior is typical of the escape rates as was found, for example, for the OVP flow [3]. The closer the sum of the columns of M to the vector $\mathbf{1}$, the larger the eigenvalue, and the transient time is determined by l,m,k and the relative sizes of the s_i's.

(iii) Assuming that $\hat{W} = W$ (so that the map is invariant under reversal of time and 90° rotation) the asymptotic stretching rate is given by

$$\log\left(\frac{\lambda_{T_{l,m,k}}}{\lambda_{W_{l,m,k}}}\right) \approx \log\left(\frac{\lambda_{T_l} + c_l \exp[-b_l(m+k)]}{\lambda_{W_l} + \exp(a_{l,m,\alpha} - b_{l,m,\alpha} k)}\right).$$

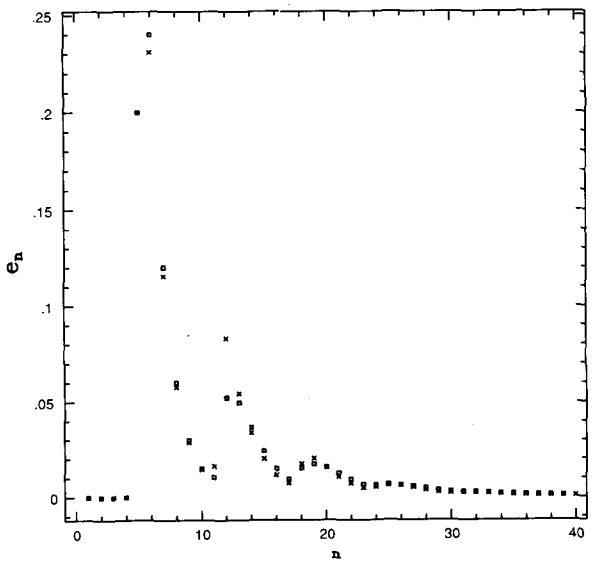

Fig. 11. The transient behavior of the escape rates. The e_n's are plotted for trellises of type 5 (□) and type $\{5,6,7,0\}$ (×) for $\alpha = 0.2$.

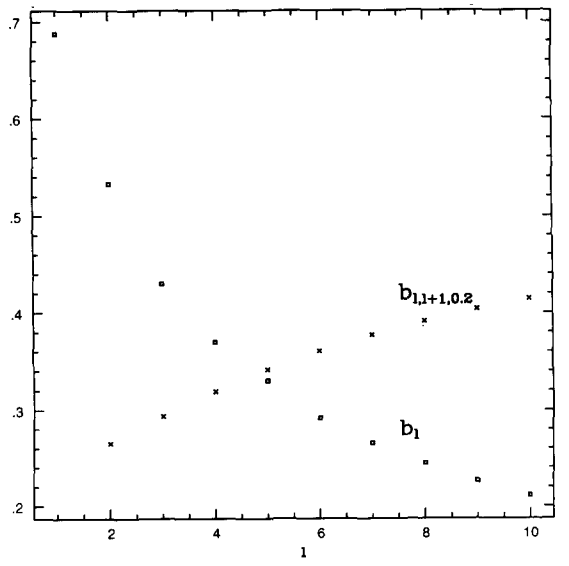

Fig. 12. The dependence of the stretching rate on l. (□) b_l and (×) $b_{l,l+1,0.2}$ versus l. For $l=4$, $b_l - b_{l,l+1,0.2}$ changes sign, resulting in a change of the asymptotic behavior of the averaged stretching rate.

As shown in fig. 12, the decay rate in k changes its behavior with l; for small l ($l < 4$ for $\alpha = 0.2$), the dominant decay rate is b_l where for large l the dominant decay rate is the $b_{l,m,\alpha}$, and for intermediate l ($l \approx 5$ for $\alpha = 0.2$) the behavior will not appear to be exponential since it is composed of a sum of comparable exponents.

To summarize, the above relations show that for m, k sufficiently large quantitative characteristics of the type-l trellis and the type-$\{l, m, k, 0\}$ trellises are exponentially close to each other. Hence we conjecture that the quantitative characteristics of other trellises which are sufficiently close to the type-$\{l, m, k, 0\}$ trellises are reasonably approximated by the quantitative characteristics of the type-$\{l, m, k, 0\}$ trellises. Specifically, if the trellises are obtained from a one-parameter family of diffeomorphisms, in a neighborhood of the type-l and the type-$\{l, m, k, 0\}$ trellises the properties of these trellises provide a good approximation to the properties of the trellis of the map.

8. Probabilistic approach – Markov chains

As was pointed out in sections 3 and 5 the extended weighted transition matrix M can be viewed as the canonical probability matrix of a Markov process, where the analog between area distribution and probabilities is natural. It is important to realize that the answer to the original question we posed in this and the previous works – given an initial uniform distribution of particles in the region S, what portion of them remains in S after n iterates of the map – was answered without the need of the probabilistic approach which necessarily relies on further assumptions regarding the map. However, this approach can be used to answer different types of questions which are concerned with the fate of a "typical" initial condition (or a specific ensemble) originating in one of the states or in S.

From the form of M and the known results regarding the Markov chains, the probable fate of a particle placed initially in one of the states can be found easily, and the relevant results will be discussed shortly. To determine the fate of a particle placed in S we need to find the probability of a particle in S to be contained in a state s. This probability is proportional to the area associated with the state s. Since the states are completely covered by images of the lobe E their areas are given by

$$\mu(s) = \sum_{n=1}^{\infty} a^n(s), \quad s > 2,$$

where $a^n(s)$ is the s component of the area vector of the nth image of the lobe E, and as was shown in sections 3 and 5 it can be approximated by $a^1 \cdot M^n$, where the nonvanishing terms of a^1 are

$$a^1(l+1) = e_1, \qquad a^1(2l+1) = \mu(E) - e_1$$

for the type-l trellis and

$$a^1(l+1) = d_1, \qquad a^1(2l+m+k+1) = d_2, \qquad a^1(3l+m+k+1) = d_3, \qquad a^1(l+m+1) = d_4$$

for trellis of type $\{l, m, k, 0\}$. Denoting by Q the submatrix of M which does not include the state g_0

(crossing out the first row and column of M) and cutting off the first term in a^1 we obtain

$$\mu(s) = a^1 \sum_{n=1}^{\infty} Q^n(s) = a^1 (I - Q)^{-1}(s), \quad s > 1. \tag{36}$$

Since the images of E cover, at the limit of infinitely many iterations, any of the D lobes and by reversing time the preimages of D cover the E lobes we conclude that the parts of S which are not contained in any of the images of the lobe E belong to the invariant set and its area can be found by subtracting from $\mu(S)$ the area of all the other states (except g_0 and g_1). Hence the area of the invariant set can be estimated by

$$\mu(\text{Inv}) = \mu(S) - \sum_{s=2}^{N} a^1 (I - Q)^{-1}(s), \tag{37}$$

where $N = 2l + 2$ for the type-l trellises and $N = 3l + 2m + k + 1$ for the type-$\{l, m, k, 0\}$ trellises. The probability of an initial condition in $\{S - \text{Inv}\}$ to belong to the state s is given by

$$p(s) = \mu(s) / [\mu(S) - \mu(\text{Inv})].$$

From the form of the matrix M we conclude that the states h_i, f_i are transient states and the g_i's belong to an absorbing chain. It is shown in Kemeny and Snell's book [21] that the following quantities can be found by simple matrix operations on the submatrices of M (W, R and L):

(1) The mean and variance of the number of times a particle starting in a transient state s_1 will visit another transient state s_2.

(2) The mean and variance of the number of iterates a particle starting in the transient state s stays in the transient chain (hence in S).

(3) The probability that a process starting at the transient state s ends up in the element of the absorbing chain t.

Combining the second and third results together with eq. (36) one can compute the mean and variance of the number of iterates a particle which started in the "stochastic layer" (S – {the invariant set}) stays in it. To get a better statistical description of the motion in this layer one should exclude, in addition to the invariant set, the first few preimages of the lobe D, which usually create a very apparent and ordered structure which will skew the statistics. Technically, this is done by replacing a^1 with a^n in eqs. (36) and (37) for some small n. We note that the resulting probability of escape at cycle k (for $k > n$) is given by

$$p_{\text{esc}}(k) = \sum_{t=1}^{l+m} \sum_{s=l+m+1}^{3l+2m+k} p(s)\, Q^{k-t+1}(s,t).$$

This should give a considerable improvement on the previously suggested probability [4] of escape given by the area of the lobe D divided by the area of the stochastic layer.

Another interesting application of the relation between the formulation of the escape rates and Markov chains is the construction of a diffusion equation. There are numerous attempts to describe the motion of particles in phase space via a diffusion equation. The classical approach for deriving such an equation is to consider the map itself as a Markov process [5], which leads to a reasonable approximations only when there are no visible island chains. When phase space is not completely ergodic, the

description of the motion of particles in the phase space as a diffusion process is misleading [4], since particles are tunneled to specific regions in phase space in a manner which does not resemble diffusive process. Escande [6] suggested incorporating the two approaches by a quasilinear approximation to the diffusion rate which is based on the lobe area. Dana et al. [24] suggested a diffusion model between islands of resonances. The current work suggests that the appropriate diffusion equation describes the diffusion between the states, where the starting and ending point are the lobes E and D, respectively, which can be located precisely in phase space, where the other states can only be roughly located.

9. Transport rates for flows

So far we have dealt with the topological structure of the trellis without any assumptions, nor specification, of the diffeomorphism it represents. In applications one is confronted with a map or an ODE and one has to determine both the type of trellis and the various parameters (such as the s_i and the d_i) from these equations. In general one needs to compute and plot the first few arcs K_n, K_n', J_n, J_n' to determine these parameters. This can be done quite easily for a given dynamical system but can become extremely time consuming if one is interested in a family of diffeomorphisms, as is the common case. We show that the use of the Whisker map provides a method for approximating all these quantities when the diffeomorphism is given by the Poincaré map of an integrable Hamiltonian system perturbed by a time-periodic perturbation. Its limitation is that one gets only an approximation of these parameters and that it applies only to the near-integrable cases.

Chirikov [14] introduced the Whisker map in 1979 paper to investigate the properties of the stochastic layer of the periodically forced pendulum and of the standard map. Lichtenberg and Lieberman [5], who call this map the separatrix map, have further investigated its implications on the stochastic layer. Escande [6] has shown that one can use this map to estimate interesting quantities such as the first retrapping time and the first retrapping area, and was the first to relate the results of the Whisker map to the transport rates in the Poincaré map.

The Whisker map was first constructed for the periodically forced pendulum; however, the procedure is quite general and can be applied to any one-degree-of-freedom Hamiltonian with homoclinic loop which is perturbed by a time-periodic Hamiltonian (generalizations to higher dimensions and to the non-Hamiltonian case are possible). Weiss and Knobloch [2] indeed used the idea of the Whisker map to model the transport near the separatrices of a two-dimensional flow which is periodic in space and contains heteroclinic connections forming a homoclinic loop.

The approach taken by all the preceding authors of replacing the dynamics of the original ODE by the approximating map is far from being justified; indeed the map approximates the flow correctly for one iterate of the map, but the accumulating error is expected to be large since the map and the flow are chaotic. The arm waving argument that since both are chaotic they should produce, at least statistically, the same answer was not established and does not seem to be correct in general.

We use the Whisker map only for limited number of iterations. The accumulating errors is shown to be bounded for these iterations hence we do not rely on the vague idea of "statistically" correct approximation but rather on an asymptotic expansion in the small parameter. Since in all the above papers the exact derivation and error estimates were not written explicitly, we start by deriving the Whisker map. Then we derive from it estimates to the various quantities such as the type numbers (l, m, k), the first few escape rates (e_n) and the stretching coefficients (s_i).

9.1. Derivation of the Whisker map

To derive the Whisker map we assume that the perturbed Hamiltonian is of the form

$$h(q,p,t) = h_0(q,p) + \epsilon h_1(q,p,t) + \mathcal{O}(\epsilon^2), \qquad h_1(q,p,t) = h_1(q,p,t+T),$$

where the origin is assumed to be the hyperbolic fixed point which, for $\epsilon = 0$, is connected to itself by a homoclinic orbit $\gamma(t)$. With no loss of generality we will assume that $\gamma(0) = (q_0, 0)$ and that the Hamiltonian is already in a form so that

$$h_0(q,p) = \tfrac{1}{2}p^2 - \tfrac{1}{2}q^2 + \text{higher-order terms}, \quad p,q \ll 1,$$
$$h_1(0,0,t) = 0. \tag{38}$$

As shown in the derivation, it is crucial to put the Hamiltonian in this form so that $h(0,0,t) = 0$ for all t. We assume that the stable and unstable manifolds of the origin intersect each other transversely when $\epsilon \neq 0$, forming a trellis in the Poincaré section $\Sigma_0 = \{(q,p,t) | t = 0\}$. This assumption can be verified analytically by computing the Melnikov's function [16, 17, 25].

The solution to the ODEs associated with this Hamiltonian, $x(t) = (q(t), p(t))$, can be transformed via a canonical transformation to the variables $(h(p(t), q(t), t), t(q(t), p(t)))$. The Whisker map is the return map for these two variables on two distinct Poincaré sections Σ_h and Σ_{t^*}, respectively. These sections are defined as follows (see fig. 13):

$$\Sigma_{t^*} = \{(q,p) | p = 0 \text{ and } |q - q_0| < \alpha\epsilon\},$$
$$\Sigma_h = \{(q,p) | [p = 0 \text{ and } 0 \le q < \alpha\epsilon] \text{ or } [q = 0 \text{ and } |p| < \alpha\epsilon]\},$$

where α is a constant of order 1. Using the evolution equations for h and t and the canonical transformation between these variables and (q, p) we can define the following two maps:

$$P^*: \Sigma_{t^*} \to \Sigma_{t^*},$$
$$(h(0, q(t^*), t^*), t^*(0, q(t^*))) \to (h(0, q(t^* + T^*), t^* + T^*), t^* + T^*),$$

where T^* is the return time of the Poincaré map P^*. Similarly,

$$P: \Sigma_h \to \Sigma_h,$$
$$(h(t), t) \to (h(t+T), t+T),$$

where T is the return time of the Poincaré map P, and the implicit dependence on q, p is suppressed from now on.

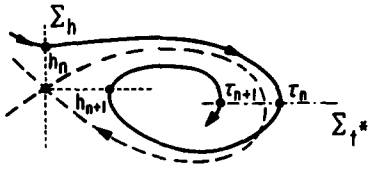

Fig. 13. The geometry of the Whisker map. (---) Unperturbed separatrices; (———) an orbit.

The Whisker map is defined in terms of these two maps to be

$$W: (h(t), t^*) \to (h(t+T), t^* + T^*).$$

In other words, letting $t < t^*$, define

$$h_n = h(t), \qquad h_{n+1} = h(t+T),$$
$$\tau_n = t^*, \qquad \tau_{n+1} = t^* + T^*.$$

This map is the exact Whisker map and it is defined in terms of the exact solutions to the perturbed ODEs. To obtain an explicit map one has to approximate these solutions by the unperturbed solutions. The jump in the energy is obtained by approximating the perturbed orbit by the unperturbed homoclinic orbit, shifted to match the phase τ_n. The return time is obtained by approximating the perturbed orbit by an unperturbed periodic orbit of the appropriate energy level. Performing this calculation for the energy jump gives

$$\begin{aligned} h_{n+1} - h_n &= \int_{t_n}^{t_{n+1}} \frac{\mathrm{d}h}{\mathrm{d}t} \left[\gamma(t - t_n^*) + \epsilon x_1(t, t_n^*) + \mathcal{O}(\epsilon^2), t\right] \mathrm{d}t \\ &= \int_{t_n - t_n^*}^{t_{n+1} - t_n^*} \frac{\mathrm{d}h}{\mathrm{d}t} \left[\gamma(t), t + t_n^*\right] \mathrm{d}t + \epsilon \int_{t_n - t_n^*}^{t_{n+1} - t_n^*} \frac{\mathrm{d}}{\mathrm{d}t} \left[\nabla h \cdot x_1(t + t_n^*, t_n^*)\right] \mathrm{d}t + \mathcal{O}(\epsilon^2) \\ &= h(\gamma(t), t_n + t_n^*)\big|_{t_n - t_n^*}^{t_{n+1} - t_n^*} + \epsilon \int_{t_n - t_n^*}^{t_{n+1} - t_n^*} \frac{\mathrm{d}}{\mathrm{d}t} \left\{\nabla h \cdot \left[x_1^{u,s} + (x_1 - x_1^{u,s})\right](t + t_n^*)\right\} \mathrm{d}t + \mathcal{O}(\epsilon^2) \\ &= \epsilon M(t_n^*) + \mathcal{O}(\epsilon h_n, \epsilon h_{n+1}, \epsilon^2), \end{aligned} \tag{39}$$

which shows that as long as $h_n = \mathcal{O}(\epsilon)$ the approximation is valid. The above derivation shows that the condition $h(0, 0, t) = 0$ for all t is essential for the convergence of the above integral.

The energy level $\hat{h}$ of the unperturbed orbit which spends the same amount of time near the fixed point as the perturbed orbit is determined by the relation

$$q_{\min}|_{h_0(q_{\min}, 0) = \hat{h}} = q_{\min}|_{h(q_{\min}, 0, t_{n+1}) = h_{n+1}} = q(t_{n+1}), \tag{40}$$

which in general implies that $\hat{h} = \hat{h}(h_{n+1}, t_{n+1})$. Using $\hat{h}$ to determine the unperturbed orbit $x_0(t)$ by requiring that $x_0(t_{n+1}) = (q_{\min}(\hat{h}), 0)$ we obtain

$$\begin{aligned} \tau_{n+1} - \tau_n &= \int_{q(t_n^*)}^{q(t_{n+1}^*)} \left(\frac{\partial h}{\partial p}\right)^{-1} \left[x_0(t) + \epsilon x_1(t)\right] \mathrm{d}q \\ &= \int_{q(t_{n+1}) - \delta}^{q(t_{n+1}) + \delta} + \int_{q(t_n^*)}^{q(t_{n+1}) - \delta} + \int_{q(t_{n+1}) + \delta}^{q(t_{n+1}^*)} \left(\frac{\partial h}{\partial p}\right)^{-1} \left[x_0(t) + \epsilon x_1(t)\right] \mathrm{d}q \\ &= 2\int_{q(t_{n+1})}^{q(t_{n+1}) + \delta} + \int_{q(t_n^*)}^{q(t_{n+1}) - \delta} + \int_{q(t_{n+1}) + \delta}^{q(t_{n+1}^*)} \left(\frac{\partial h_0}{\partial p}\right)^{-1} x_0(t) \, \mathrm{d}q + \mathcal{O}(\epsilon) \\ &= T(\hat{h}) + \mathcal{O}(\epsilon), \end{aligned} \tag{41}$$

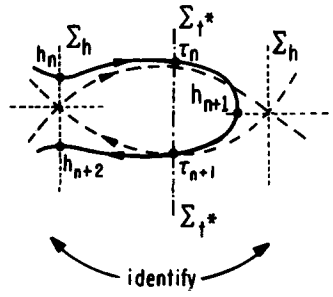

Fig. 14. The geometry of the original Whisker map. (---) Unperturbed separatrices; (———) an orbit.

where $T(\hat{h})$ is the period of the unperturbed orbit $x_0(t)$.

If one requires that $h(q,0,t_{n+1}) = h_0(q,0)[1+\mathcal{O}(\epsilon)]$ (as is the case in the periodically forced pendulum) eq. (40) implies that $\hat{h} = h_{n+1}[1+\mathcal{O}(\epsilon)]$, which leads, together with eqs. (39) and (41) to the Whisker map:

$$\begin{aligned} h_{n+1} &= h_n + \epsilon M(\tau_n) + \mathcal{O}(\epsilon^2), \\ \tau_{n+1} &= \tau_n + T(h_{n+1}) + \mathcal{O}(\epsilon), \end{aligned} \tag{42}$$

where $M(t)$ is the Melnikov function [16–18, 25] and $T(h)$ is the period of the unperturbed orbit with energy h. If h_{n+1} is positive, the particle escapes to infinity and the return time is not defined. The geometry for which this map was first constructed, the forced pendulum, is as depicted in fig. 14 and the construction of the map is similar (in this case the map is defined for all h's).

Note that multiple application of this map will necessarily lead to accumulating errors, which must be taken into account. Specifically, denoting by $\mathrm{er}(h_n), \mathrm{er}(t_n)$ the accumulating errors in h and τ respectively after the nth iteration of the map, we obtain the following difference equation for them:

$$\begin{aligned} \mathrm{er}(h_{n+1}) &= \mathrm{er}(h_n) + \epsilon M'(\tau_n)\,\mathrm{er}(t_n) + a\epsilon^2, \\ \mathrm{er}(t_{n+1}) &= \mathrm{er}(t_n) + T'(h_{n+1})\,\mathrm{er}(h_{n+1}) + b\epsilon, \end{aligned} \tag{43}$$

where a and b are the coefficients of the higher-order terms neglected in the Whisker map approximation, and are assumed to be bounded. The homogeneous error equation is exactly the linearization of the Whisker map, hence the homogeneous solution to the error equations grows with exponential growth rate, which is equal to the largest Lyapunov exponent of the Whisker map. Moreover, a sudden burst of the error may happen since $T'(h) \to \infty$ as $h \to 0$, hence, once an orbit passes too close to the separatrix the approximation breaks down! (Escande [6] had addressed this problem in the adiabatic limit by introducing a more complicated map.) These considerations imply that the Whisker map cannot be used to replace the dynamics of the *ODE* it approximates for all initial conditions or for many iterations. Eqs. (43) supply a method for testing whether an individual approximation is valid. We note that the blowup of the error term in τ_n supports the "ensemble" approach which assumes randomization of the phase. However, the growth in $\mathrm{er}(h_n)$ is not handled by this approach, and further investigation regarding this effect are needed.

9.2. Determination of the type number

To obtain the type number of the trellis in the Poincaré section Σ_0 we identify the initial conditions in the lobe E in terms of their h_0, h_1 and τ_0 values, and then impose the homoclinicity condition $h_2 = 0$. The resulting return time τ_1 and the number of distinct solutions determine the type number l and the existence of finite m and k.

The points in the lobe E are characterized by the following three conditions:

$$\text{(i) } h_0 \geq 0, \quad \text{(ii) } h_1 \leq 0, \quad \text{(iii) } 0 \leq \tau_0 \leq T, \tag{44}$$

where T is the period of the Melnikov function (and of h_1). The unstable (stable) boundary of E is given by the points which satisfy the three conditions in (44) and $h_0 = 0$ ($h_1 = 0$). The type number is determined by the number of solutions τ_0 to the following set of equations:

$$0 \leq \tau_0 \leq T, \quad h_0 = 0, \quad h_1 < 0, \quad h_2 = 0, \quad \tau_1 \geq lT. \tag{45}$$

In general there will be a minimal l for which the above equation has solutions, and this is exactly the type number l. Eqs. (45) attain typically no solutions, two or four solutions (and at the bifurcation points one and three solutions which indicate tangencies nearby in parameter space). When exactly two solutions are found, m, k can be taken to be infinite and the trellis can be approximated by a type-l trellis. In the neighborhood of the bifurcation from two to four solutions m, k are finite but large, hence, by the previous discussion the trellis can still be approximated by the type-l trellis. Farther from the bifurcation point, where (45) has the four ordered solutions τ_0^i, $i = 1, \ldots, 4$ the trellis can be approximated by a type-$\{l, m, k, 0\}$ trellis, where m and k are still needed to be determined. Using the same arguments as above, we find that m will be determined as the minimal integer for which the following equations attain solutions τ_0:

$$\tau_0^2 \leq \tau_0 \leq \tau_0^3, \quad h_0 = 0, \quad h_1 < 0, \quad h_2 < 0, \quad h_3 = 0, \quad \tau_2 \geq mT. \tag{46}$$

This set of equations typically attains an even number of solutions. The type-$\{l, m, k, 0\}$ trellis corresponds to the case of exactly two solutions, and can be used in the neighborhood of this case. When more intersections occur one has to consider trellises of other types. The determination of k is done in a similar fashion by considering the inverse map on the lobe D, and will not be presented here.

The number of iterates of the Whisker map needed to compute l and m are 2 and 3, respectively, and in both cases only the energy estimate is needed for the last iterate. Using eqs. (43) we find that the accumulating errors depend on the magnitude of $T'(h_1)$ and $T'(h_2)$ (assuming the derivatives of M can be bounded, which is the common case). While it is reasonable to assume that h_1 is large enough for the errors to stay small, the value of h_2 may be too small (for example, when m is very large) leading to large errors. This difficulty is to be expected since the J_{-m}'s accumulate along J_0 as $m \to \infty$ and their width decreases exponentially with m, hence a regular perturbation method cannot resolve the exact m. However, it follows from the previous section that for large m one can simply replace m by ∞ for all practical purposes. The moral from this consideration is that in any case these error estimates must be performed in each case to verify the validity of the approximation, and that in general one expects the estimates for l to be accurate and the estimates for small m to be valid (and similarly for small k).

9.3. Determination of the initial escape rates and the weights

The idea that the Whisker map can be used to compute the escape rates was first suggested by Escande [6], who estimated the first retrapping portion, e_l for the forced pendulum. Weiss and Knobloch [2] have used the Whisker map to numerically evolve initial conditions, determining whether a particle is trapped or not by the sign of h. Both have suggested to use this map to investigate the long-time behavior of the transport. Here we use the Whisker map only to determine the characteristics of the first few iterates, taking into consideration the fast growth of the accumulating errors.

To determine the portion of E which escapes after n iterations one has to solve the following set of equations:

$$0 \le \tau_0 \le T, \qquad h_0 = 0,$$

$\exists n_1 < n$ such that

$$h_j < 0, \quad \text{for } 1 \le j \le n_1, \qquad h_{n+1} > 0, \qquad (n-1)T \le \tau_{n_1} < nT.$$

This set of equations can be solved analytically for $n \le 2l$ (since $n_1 = 1$ in this case) and, though technically more difficult, for small $n - 2l$. We note that the error estimates become worse for larger n_1, and even for small n_1 one should be cautious when dealing with the boundaries. Using the above equations one can determine the escape rates $e_l, \ldots, e_{2l+1}$, and for the type-l trellises these can be used to determine the stretching weights s_i as follows. Let I denote the area of the lobe E which can be approximated by [3]

$$I = \epsilon \int_{t_0}^{t_1} M(t)\, \mathrm{d}t + \mathcal{O}(\epsilon^2)$$

and let $w = I - e_l$. Then, from the form of the matrix M in section 3 we find that for $l > 2$:

$$e_{l+1} = (1 - s_1 - s_2)w, \qquad e_{l+2} = ws_1(1 - s_1 - s_2), \qquad e_{2l+1} = ws_1^l(1 - s_1 - s_2) + ws_2(1 - s_3 - s_4),$$

hence

$$s_1 = \frac{e_{l+2}}{e_{l+1}}, \qquad s_2 = 1 - \frac{e_{l+1}}{w} - \frac{e_{l+2}}{e_{l+1}}, \qquad s_3 + s_4 = 1 - \frac{e_{2l+1} - s_1^l e_{l+1}}{ws_2}.$$

Similar considerations will supply estimates for the weights in the type-$\{l, m, k, 0\}$ trellises.

10. Conclusions

In sections 2–6 we have developed a method for estimating the escape rates, the manifold length and the topological entropy for the type-l and the type-$\{l, m, k, 0\}$ families of diffeomorphisms. In section 7 we have shown that many properties of the type-$\{l, m, k, 0\}$ diffeomorphisms can be approximated by the properties of the type-l diffeomorphisms for sufficiently large m, k. This suggests that the topological structure of the trellis of a diffeomorphism can serve as a skeleton for approximating these quantities.

The validity of the semi-linear approximation, used in sections 3 and 5 to approximate the escape rates, is yet to be verified; a subsequent paper will be devoted to a numerical investigation of transport in a specific example and the proposed methods will be tested. We note that other work [7] has concentrated on the improvement of the semi-linear approximation of the escape rates for nonlinear maps, hence, in any case, the combination of these two works gives an adequate method for estimating the escape rates for a large family of diffeomorphisms.

In section 8 we have linked the formalism of the weighted transition matrices with finite Markov chains, computed the area associated with each state, the area of the invariant set and the escaping probability and suggested a different method for constructing a diffusion equation.

In section 9 we constructed an analytical method for determining the type of trellis associated with a time-periodic flow. In the process, we have derived the equations for the accumulating errors associated with the Whisker map. We have shown that one can use this map to obtain the important parameters which are needed for the computation of the escape rates, namely the type number, the stretching rates and the initial escape rates. Hence a complete approximation scheme for the computation of the escape rates for periodically perturbed Hamiltonian systems (which satisfy some geometrical assumptions) was presented.

Acknowledgements

I would like to thank L.P. Kadanoff for many helpful suggestions and S. Wiggins for his constructive comments. I have also benefitted from discussions with P. Gaspard, G. Gunaratne and M. Shelley. This work is supported by NSF grant DMS8903244 and by the Office of Naval Research.

Appendix. Formal definition of the type-$\{l, m, k, 0\}$ trellises

We define the type-$\{l, m, k, 0\}$ trellises, described by their geometrical properties in section 4, formally. We then use this definition to prove that two type-$\{l, m, k, 0\}$ trellises are weakly equivalent and therefore that they are well defined.

Denote the following statements by (s1), (s2), (s3) and (s4):

(s1) If a, b are two $<_u$ adjacent points of h_n and $t(a) = t(b)$ then $U[a, b]$ is contained in $D_{-t(a)}$.

(s2) If a, b are two $<_u$ adjacent points of h_n and $t(a) < t(b)$ then $h_{n+1} \cap U(a, b)$ contains exactly two points whenever $t(a) \leq n - l$ and is empty whenever $t(a) > n - l$.

(s3) If a, b are two $<_u$ adjacent points of h_n and $t(a) = t(b)$ then $h_{n+1} \cap U(a, b)$ contains exactly two points when $t(a) = n - m + 1$ and is empty when $t(a) > n - m + 1$.

(s4) If a, b are two $<_u$ adjacent points of h_n, $t(a) = n - l$ and $t(a) < t(b)$ then $h_{n+1} \cap U(a, b)$ contains four homoclinic points, q_i, $i = 1, \ldots, 4$, where $\{q_1, q_2\}$ and $\{q_3, q_4\}$ satisfy (s1) and $\{q_2, q_3\}$ satisfy (s3). If $n = l + k - 1$ and $b <_u a$ then $q_1 = q_2$, namely there are only three new homoclinic points created as depicted in fig. 5.

Recall that all the homoclinic points in K_0 of a type-l trellis satisfy either (s1) or (s2). For the extension, homoclinic points will be distinguished by four neighbors instead of only two, resulting in four different options for their behavior.

We define the $\{l, m, k, 0\}$ trellis inductively, where the initial development is given explicitly for $n \leq k + l - 1$ and inductively for larger n. Let $h_n = \{q_0, r_1, \ldots, r_p, p_1\} = \{r_0, r_1, \ldots, r_p, r_{p+1}\}$ where

$r_i <_u r_{i+1}$. Let $a(i)$ denote the first homoclinic point (with respect to the unstable ordering, as above) in h_n with type number i, and by $b(i)$ the last homoclinic point in h_n of type i, for all $i > 0$. The $a(i)$'s and $b(i)$'s are independent of n for all $i \le n$.

Hypothesis C0:

(i) For $0 < n < l$, $h_n = \{q_0, p_1\}$.

(ii) For $n = l$, $h_n = \{q_0, a(l), A, B, b(l), p_1\}$, the pairs $\{a(l), A\}$ and $\{B, b(l)\}$ satisfy (s1), and the pair A, B satisfies (s3).

(iii) For $l < n < k + l$ all the homoclinic points which are not contained in $[A, B]$ satisfy either (s1) or (s2). If $m < k$, (s3) implies that two homoclinic points are created in $U[A, B]$ for $n = l + m$, and for $n > l + m$ all points in K_0 satisfy either (s1) or (s2).

(iv) For $l + k \le n$, $\{a(n - l + 1), a(n - l)\}$ and $\{b(n - l), b(n - l + 1)\}$ satisfy (s4), and all other points are determined by (s1) and (s2) or, in case they were created by (s4) or given by $\{A, B\}$, by (s3).

More precisely, given $h_n (n \ge l + k - 1)$ one can construct h_{n+1} as follows:

(1) If $t(r_i) \ne t(r_{i+1})$ and $r_i \notin \{a(n - l + 1), b(n - l)\}$ then $\{r_i, r_{i+1}\}$ satisfy (s2).

(2) If $t(r_i) \ne t(r_{i+1})$ and $r_i \in \{a(n - l + 1), b(n - l)\}$ then $\{r_i, r_{i+1}\}$ satisfy (s4).

(3) If $t(r_i) = t(r_{i+1})$, $t(r_{i-1}) \ne t(r_i)$ and $t(r_{i+1}) \ne t(r_{i+2})$ then $\{r_i, r_{i+1}\}$ satisfy (s1).

(4) If $t(r_i) = t(r_{i+1}) = t(r_{i+2})$, $t(r_{i-1}) \ne t(r_i)$ and $t(r_{i+3}) \ne t(r_{i+2})$ then $\{r_i, r_{i+1}\}$ satisfy (s3) and $\{r_{i+1}, r_{i+2}\}$ satisfy (s1).

(5) If $t(r_i) = t(r_{i+1}) = t(r_{i+2}) = t(r_{i+3})$, then $\{r_i, r_{i+1}\}$, $\{r_{i+2}, r_{i+3}\}$ satisfy (s1) and $\{r_{i+1}, r_{i+2}\}$ satisfy (s3).

Definition 4.1. A trellis which satisfies hypotheses A, B and C0 is called a trellis of type $\{l, m, k, 0\}$.

Theorem 4.1. Two trellises of type $\{l, m, k, 0\}$ are weakly equivalent.

Proof. The proof is a modification of Easton's proof that two type-l trellises are weakly equivalent.

Let τ, τ^* be two trellises of type $\{l, m, k, 0\}$, and let τ_n, τ_n^* denote their developments, e.g.

$$\tau_n = W^u_- \cup W^s_- \cup U[p, p_n] \cup S[p, p_{-n+1}].$$

We need to prove that for all n the developments τ_n, τ_n^* are homeomorphic with a homeomorphism which preserves the respective stable and unstable ordering.

Lemma. There exists a one-to-one correspondence g: $H \cap K_0 \to H^* \cap K_0$ which preserves the stable and unstable orderings and the type numbers.

Proof. We start by defining $g(q_0) = q_0^*$ and $g(p_1) = p_1^*$. Inductively define g by assuming that g: $h_n \to h_n^*$ has been defined and is a one-to-one correspondence which preserves the stable and unstable orderings.

Let a and b denote a pair of $<_u$ adjacent points of h_n with $U[a, b] \cap h_{n+1} \ne \emptyset$ and $t(a) \le t(b)$. By hypothesis C0 there are three cases to consider where $U[a, b] \cap h_{n+1}$ can contain two, three or four homoclinic points. Since hypothesis C0 gives an inductive construction of h_{n+1} from the previous h_n's it is clear that the number of homoclinic points in $U[g(a), g(b)] \cap h_{n+1}^*$ is the same as in $U[a, b] \cap h_{n+1}$, hence we can define g on these homoclinic points so that the unstable ordering is preserved. We now need to prove that this definition of g will also preserve the stable ordering.

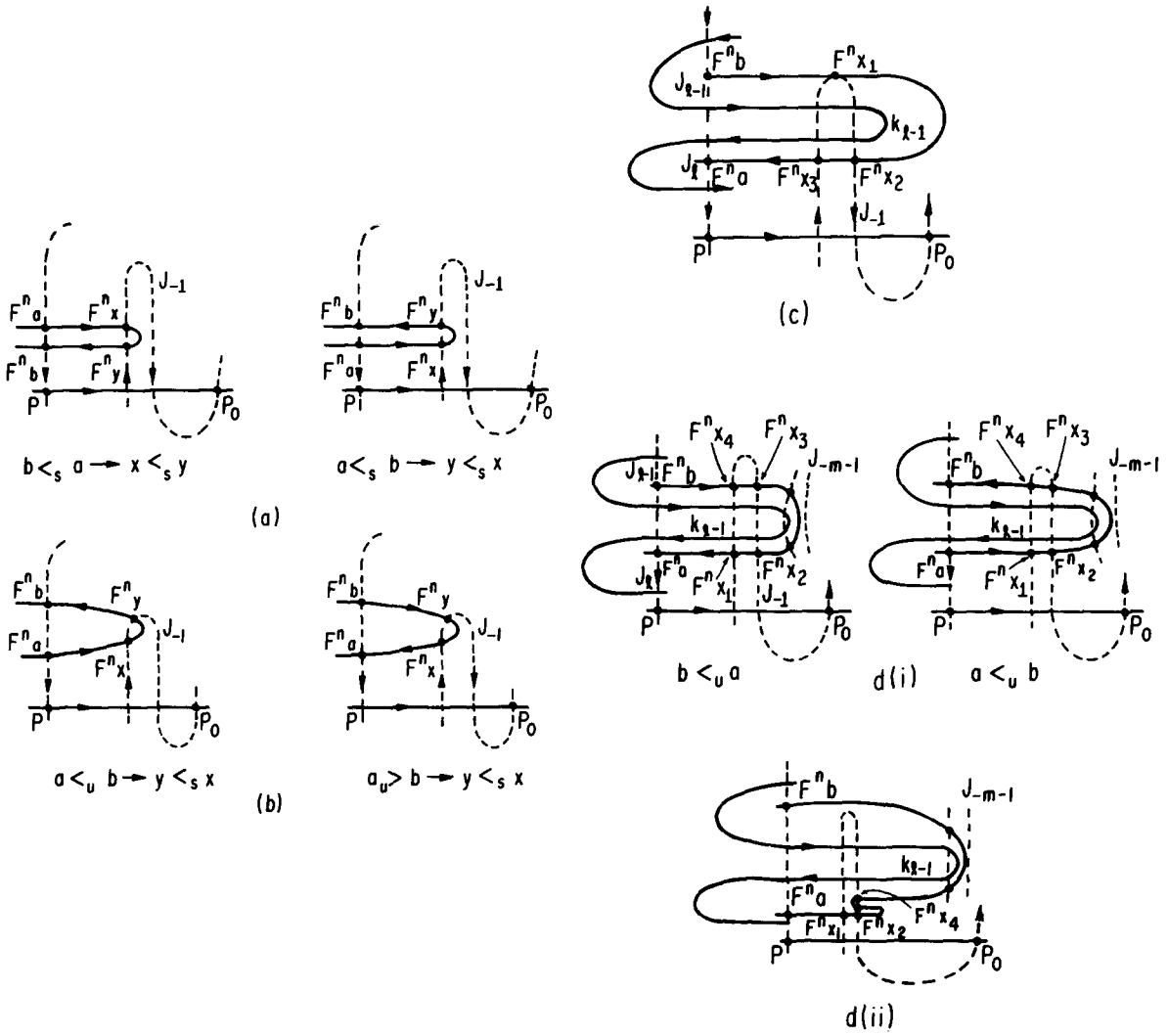

Fig. 15. Various intersections of $F^n(U[a,b])$ and J_{-1}. For details, see proof of theorem 4.1.

(i) Consider the case $t(a) = t(b)$, and let $a <_u b$. By hypothesis C0, the only nontrivial case ($U[a,b] \cap h_{n+1} \neq \varnothing$) is when $t(a) = n - m + 1$. In this case there are exactly two points $x <_u y$ in $U[a,b] \cap h_{n+1}$. Since $F^n(a)$, $F^n(b) \in J_{m-1}$ and $F^n(x)$, $F^n(y) \in J_{-1}$, and since the stable and unstable orderings are preserved under the map F, we conclude that if $a <_s b$ then $y <_s x$ and if $b <_s a$ then $x <_s y$ (see fig. 15a). Finally, by the induction hypothesis the stable ordering of a, b is preserved under g, hence the stable ordering of x, y is preserved under g.

(ii) Consider the case $t(a) < t(b)$. By C0 there are three nontrivial subcases to consider:

(a) $U[a,b] \cap h_{n+1}$ contains two homoclinic points, labeled by x, y where x is $<_u$ adjacent to a. Since $t(a) < t(b)$ we obtain that $F^n(a) <_s F^n(b)$ and since $F^n(x), F^n(y) \in J_{-1}$ we obtain that the stable ordering is determined and $y <_s x$ (see fig. 15b).

(b) $U[a,b] \cap h_{n+1}$ contains three homoclinic points, labeled by x_1, x_2, x_3 ordered by the unstable ordering. By C0, $b <_u a$ and $t(b) = t(a) + 1 = n - l + 1$, hence $F^n(a) \in J_l$ and $F^n(b) \in J_{l-1}$, and the only possible stable ordering of the x_i's is $x_2 <_s x_1 <_s x_3$ as depicted in fig. 15c.
(c) $U[a,b] \cap h_{n+1}$ contains four homoclinic points, labeled by x_1, x_2, x_3, x_4 so that x_1 is $<_u$ adjacent to a, and x_j's follow by the unstable ordering so that x_4 is $<_u$ adjacent to b. By C0, $t(b) = t(a) + 1 = n - l + 1$, hence $F^n(a) \in J_l$ and $F^n(b) \in J_{l-1}$. The only stable ordering which is allowable is given by $x_2 <_s x_3 <_s x_4 <_s x_1$ as shown in fig. (15d, i). Fig. 15d, ii illustrates the other situation which satisfies the conditions on the unstable ordering but violates C0 since $U[F^n b, F^n x_3]$ contains two additional homoclinic points and $U[x_2, x_3]$ does not necessarily satisfy (s3) as required.

To summarize, we have shown that in all the different cases the unstable ordering of the new homoclinic points determined completely their stable ordering, hence that g preserves both the stable and unstable orderings, and by its construction it also preserves the type numbers.

The extension of g from the set of homoclinic points on K_0 to the set of all homoclinic points and then to the segments connecting them follows exactly as in Easton's proof for the type-l case.

References

[1] M. Feingold, L.P. Kadanoff and O. Piro, Transport of passive scalars: KAM surfaces and diffusion in three-dimensional Liouvillian maps, in: Instabilities and Nonequilibrium Structures II, eds. P. Collet, E. Tirapegui and D. Villarroel (Kluwer, Dordrecht, 1989) p. 37.
[2] J.B. Weiss and E. Knobloch, Mass transport and mixing by modulated traveling waves, Phys. Rev. A submitted for publication.
[3] V. Rom-Kedar, A. Leonard and S. Wiggins, An analytical study of transport, mixing and chaos in an unsteady vortical flow, J. Fluid Mech.
[4] R.S. MacKay, J.D. Meiss and I.C. Percival, Transport in Hamiltonian systems, Physica D 13 (1984) 55; J.D. Meiss and E. Ott, Markov tree model of transport in area-preserving maps, Physica D 20 (1986) 387.
[5] A.J. Lichtenberg and M.A. Lieberman, Regular and Stochastic Motion (Springer, Berlin, 1983).
[6] D.F. Escande, Hamiltonian chaos and adiabaticity, in: Plasma Theory and Nonlinear and Turbulent Processes in Physics (Proc. Intl. Workshop, Kiev, 1987), eds. V.G. Bar'yakhtar, V.M. Chernovsenko, N.S. Erokhin, A.G. Sitenko and V.E. Zakharov (World Scientific, Singapore, 1988) p. 398.
[7] P. Gaspard and S.A. Rice, Scattering from a classically chaotic repellor, J. Chem Phys. 90 (1989) 2225.
[8] M.J. Davis and S.K. Gray, Unimolecular reactions and phase space bottlenecks, J. Chem. Phys. 84 (1986) 10.
[9] D. Bensimon and L.P. Kadanoff, Extended chaos and disappearance of KAM trajectories, Physica D 13 (1984) 82.
[10] V. Rom-Kedar and S. Wiggins, Transport in two-dimensional maps, Arch. Rational Mech. Anal. 109 (1990) 239.
[11] S. Wiggins, On the geometry of transport in phase space I. Transport in k-degree-of-freedom Hamiltonian systems, $2 \leq k < \infty$, Physica D, in press.
[12] R.W. Easton, Trellises formed by stable and unstable manifolds in the plane, Trans. Am. Math. Soc. 294 (1986) 2.
[13] K. Judd, The fractal dimension of a homoclinic bifurcation, preprint (1989); The fractal dimension of a homoclinic bifurcation 2: Heteroclinic orbits and the Duffing system, preprint (1989).
[14] B.V. Chirikov, A universal instability of many-dimensional oscillator systems, Phys. Rep. 52 (1979) 263.
[15] H. Poincaré, Les Methods Nouvelles de la Mechanique Celeste (Gauthier-Villars, Paris, 1892).
[16] J. Guckenheimer and P. Holmes, Non-linear Oscillations, Dynamical Systems and Bifurcations of Vector Fields (Springer, Berlin, 1983).
[17] S. Wiggins, Global Bifurcations and Chaos – Analytical Methods (Springer, Berlin, 1989).
[18] R.L. Devaney, An Introduction to Chaotic Dynamical Systems (Addison–Wesley, New York, 1987).
[19] J.M. Finn and E. Ott, Chaotic flows and magnetic dynamics, Phys Rev. Lett. 60 (1988) 9.
[20] P. Grassberger and I. Procaccia, Physica D 13 (1984) 34.
[21] J.C. Kemeny and J.L. Snell, Finite Markov Chains, (Springer, Berlin, 1983); W. Feller, An Introduction to Probability Theory and Applications (Wiley, New York, 1968).
[22] A. Leonard, V. Rom-Kedar and S. Wiggins, Fluid mixing and dynamical systems, Proceedings of the International Conference on 'The Physics of Chaos and Systems Far from Equilibrium,' Nuc. Phys. B (Proc. Suppl.) 2 (1987) 179.
[23] D.V. Khakhar, H. III Rising and J.M. Ottino, Analysis of chaotic mixing in two model systems, J. Fluid Mech. 172 (1986) 419.
[24] I. Dana, N.W. Murray and I. Percival, Resonances and diffusion in periodic Hamiltonian maps, Phys. Rev. Lett. 62 (1989) 233.
[25] V.K. Melnikov, On the stability of the center for time periodic perturbations, Trans. Moscow Math. Soc. 12 (1963) 1.